SECTION 4

HYDROSTATIC EXTRUSION CONTAINERS DESIGNED AND CONSTRUCTED IN THE PROGRAM

SECTION 4

HYDROSTATIC EXTRUSION CONTAINERS DESIGNED AND CONSTRUCTED IN THE PROGRAM

XXXII

SUMMARY OF SECTION 4

The history of container design during the course of this program essentially follows the developments described in Section 3. An early container of 3-ring construction, designed on the maximum-shear-strength failure criterion failed due to low-cycle fatigue. The liner was replaced by two shrink-fit rings to obtain a higher prestress in the bore. This container was used in the remainder of the program. Stress analyses are presented for both of those containers. In addition, this section describes the design and the construction of a container that was intended for stand-by use in the event of another fatigue failure. This container was designed on the basis of fatigue design described in Section 3.

XXXIII

ANALYSIS OF THREE CONTAINERS DESIGN

The configuration of the three hydrostatic-extrusion containers described herein was basically as shown in Figure 66. The boundary conditions for the designs were:

(1) Maximum operating internal pressure on bore = 250,000 psi

(2) Maximum operating temperature = 500 F

(3) Pressure vessel ID = 2.375 inches

(4) Pressure vessel OD = 22.000 inches

(5) Axial load on vessel is negligible.

For reference purposes, the containers will be designated Containers I, II, and III in order of historical development. The design of Container I commenced in June, 1961, and was modified in January, 1965, to be redesignated Container II. As a result of the liner fatigue failure experienced with Container I, Container III was designed on the basis of a fatigue-failure criterion with the aim of obtaining a fatigue life in the order of 10^4 to 10^5 cycles. Container III was completed toward the end of the program but was not used in the hydrostatic-extrusion studies described in Sections 1 and 2.

Container I

Container I, which was designed and constructed in the previous program[47], was used in the early stages of this program. A detailed analysis of its design has been published.[47] In view of the more sophisticated analysis made in Section 3, it would be irrevelant to detail the design steps taken. However, the failure criterion used and the design interferences obtained will provide a useful background to the development of container designs.

Selection of Failure Criterion

Initially, failure of the design for Container I was interpreted as that condition where the diameter of the bore increased due to plastic yielding of the bore surface. Such a condition would have caused leakage by the previously close fitting stem that would result in an inability to compress the fluid adequately. With this in mind, three commonly applied failure criterion were examined to determine which was the most applicable.

The Rankine or maximum-normal-stress theory teaches that failure will occur when any one of the principal stresses reaches the level of the yield strength in uniaxial tension. Thus, it neglects the effects of the other two principal stresses. The Tresca or maximum-shearing-stress theory predicts yielding will occur when the difference between the maximum and minimum principal stresses reaches a level of the yield strength in simple tension. Experimental evidence suggested that this theory was on the

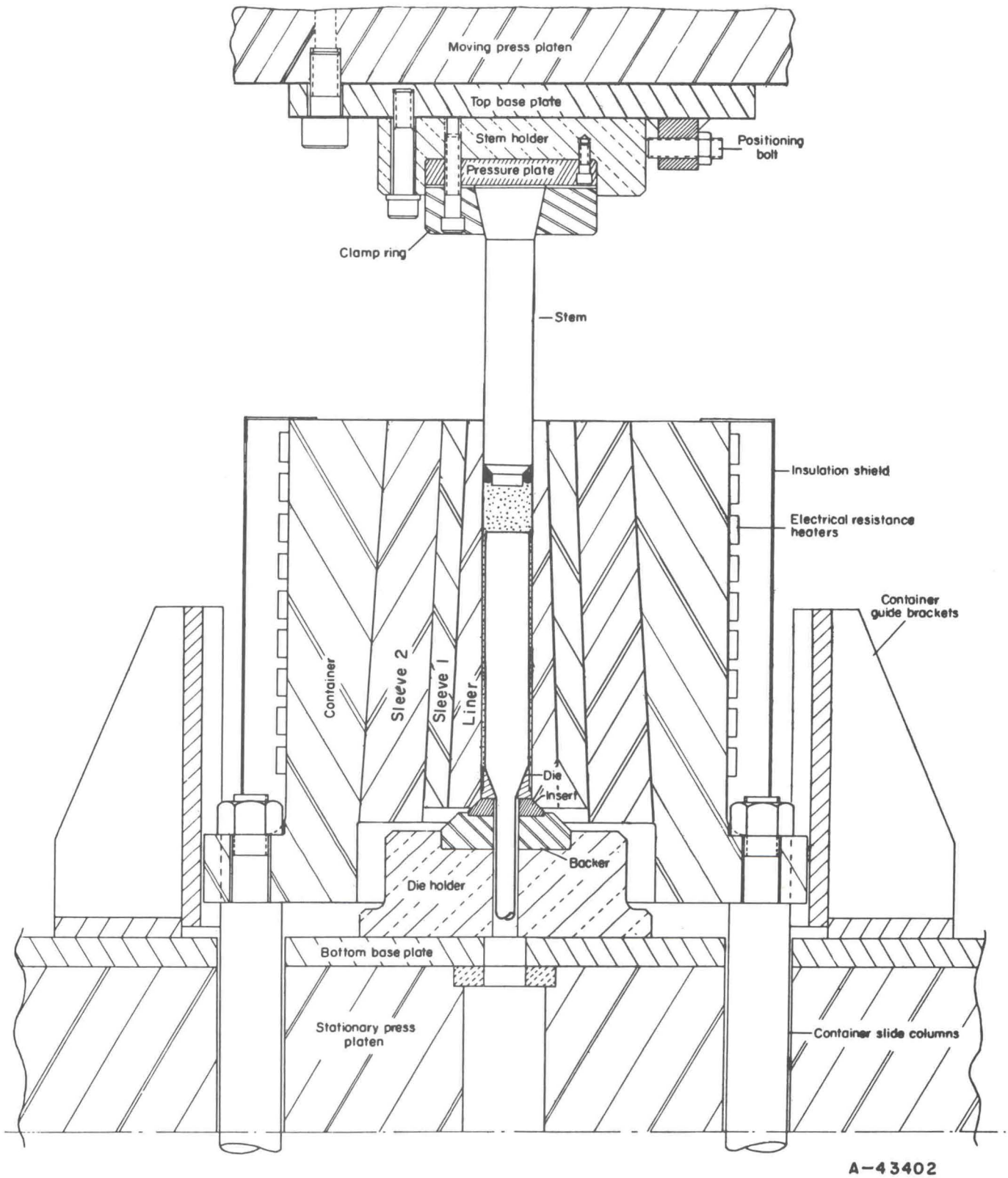

FIGURE 66. CROSS-SECTIONAL VIEW OF HYDROSTATIC-EXTRUSION TOOLING

conservative side for predicting stresses that would produce yielding in shear. Therefore, it was decided to base the container design on the Hencky-Von Mises or maximum-distortion-energy criterion.

The Hencky-Von Mises theory holds that a material subjected to a three-dimensional stress system will yield when

$$(\sigma_1 - \sigma_2)^2 + (\sigma_2 - \sigma_3)^2 + (\sigma_3 - \sigma_1)^2 = 2\,\sigma_y^2 = 6\,K^2 \quad ,$$

where

σ_1, σ_2, σ_3 = principal stresses

σ_y = yield stress as determined in uniaxial tensile or compressive tests

K = yield stress in pure shear.

In this case, for a container assembly, the stresses are considered to be biaxial because there is no axial load on the vessel. The hoop stresses are usually tensile and the radial stresses are always compressive. These two stresses will be the principal stresses because there are not externally applied shear stresses in the system. High resulting shear stresses can be expected when the system consists of two principal stresses of opposing sign.

Under biaxial conditions the Mises yield criterion becomes:

$$\sigma_1^2 - (\sigma_1\sigma_3) + \sigma_3^2 = \sigma_y^2 = 3\,K^2 \quad .$$

This equation predicts that yielding will occur when the stress in pure shear becomes equal to 0.577 Y. This value is equivalent to the maximum-shear-stress criterion provided that the yield stresses in pure tension or compression are multiplied by $2/\sqrt{3}$. With that modification of the Tresca criterion, solutions determined by either relationship agree within approximately two to six percent.

Therefore, it was decided that the container would not be expected to deform plastically, and the design would be acceptable, if the stressed metal in the vessel met either of the following equivalent limiting conditions:

Von Mises $$\frac{(\sigma_1^2 - \sigma_1\,\sigma_3 + \sigma_3^2)^{0.5}}{\sqrt{3}} < 0.577\ Y$$

Modified Tresca $$\frac{\sigma_1 - \sigma_3}{2} < 0.577\ Y$$

where

σ_1 = hoop stress at the inside of the liner

σ_3 = radial stress at the inside of the liner.

Stress Analysis of Container Assembly

To keep the tensile hoop stress on the liner bore to an acceptable minimum, the maximum shrink fit considered feasible was used between the sleeve and the liner. The shrink fit was limited by the temperature to which the sleeve could be heated without softening. This temperature was 1000 F for the alloy steel used for the sleeve. Since the liner was kept at room temperature during assembly, the maximum permissible shrink fit was 0.007 inch per inch. Although this is an extraordinarily large shrink fit for the size of the components involved, it was achieved with no apparent adverse effects. The shrink fit of the container on the sleeve was 0.0025 inch per inch. Figure 67 shows the arrangement of the rings and indicates interferences between them.

For the component dimensions, the effects of the shrink fits were as indicated in Table XLIX. These values were computed in a straight-forward manner by applying Lamé's equations for thick-walled pressure vessels. The elastic modulus was taken to be 30×10^6 psi at 80 F and 25×10^6 psi at 500 F. A step-by-step procedure was used to determine each component stress in the assembly. The resulting prestresses at various conditions of interest were then determined by super-position of the component stresses.

TABLE XLIX. PRESTRESSES DEVELOPED IN THE CONTAINER ASSEMBLY AT 80 F AND 500 F

Component	Nominal Diameter, inches	Taper, degrees	Diametral Interference, inch	Resulting Prestress at 80 F, psi		Resulting Prestress at 500 F, psi	
				Radial	Hoop	Radial	Hoop
Liner, Inside	2.375	0	--	0	-200,000	0	-166,650
Outside	7.437	2	--	-88,800	-110,200	-74,700	-91,850
			0.052				
Sleeve, Inside	7.437	2	--	-88,800	+102,000	-74,700	+85,000
Outside	13.375	3	--	-23,200	+35,750	-19,700	+29,300
			0.033				
Container, Inside	13.375	3	--	-23,200	+51,175	-19,700	+42,650
Outside	22.0	0	--	0	+27,625	0	+23,000

The hoop and radial components of the stresses developed in the container assembly solely by internal pressure, or independent of prestress, were also calculated. The values are given in Table L. The stresses resulting from the combined effects of the shrink fits and internal pressure are equal, of course, to the algebraic sums of the appropriate values in Tables XLIX and L. The resultant stresses, at various locations, are indicated on Figures 68 and 69.

TABLE L. STRESSES RESULTING SOLELY FROM AN INTERNAL PRESSURE OF 250,000 PSI

Component	Stress, psi	
	Radial	Hoop
Liner, Inside	-250,000	+255,900
Outside	-23,900	+28,750
Sleeve, Inside	-23,900	+28,750
Outside	-8,000	+10,900
Container, Inside	-8,000	+10,900
Outside	0	+5,775

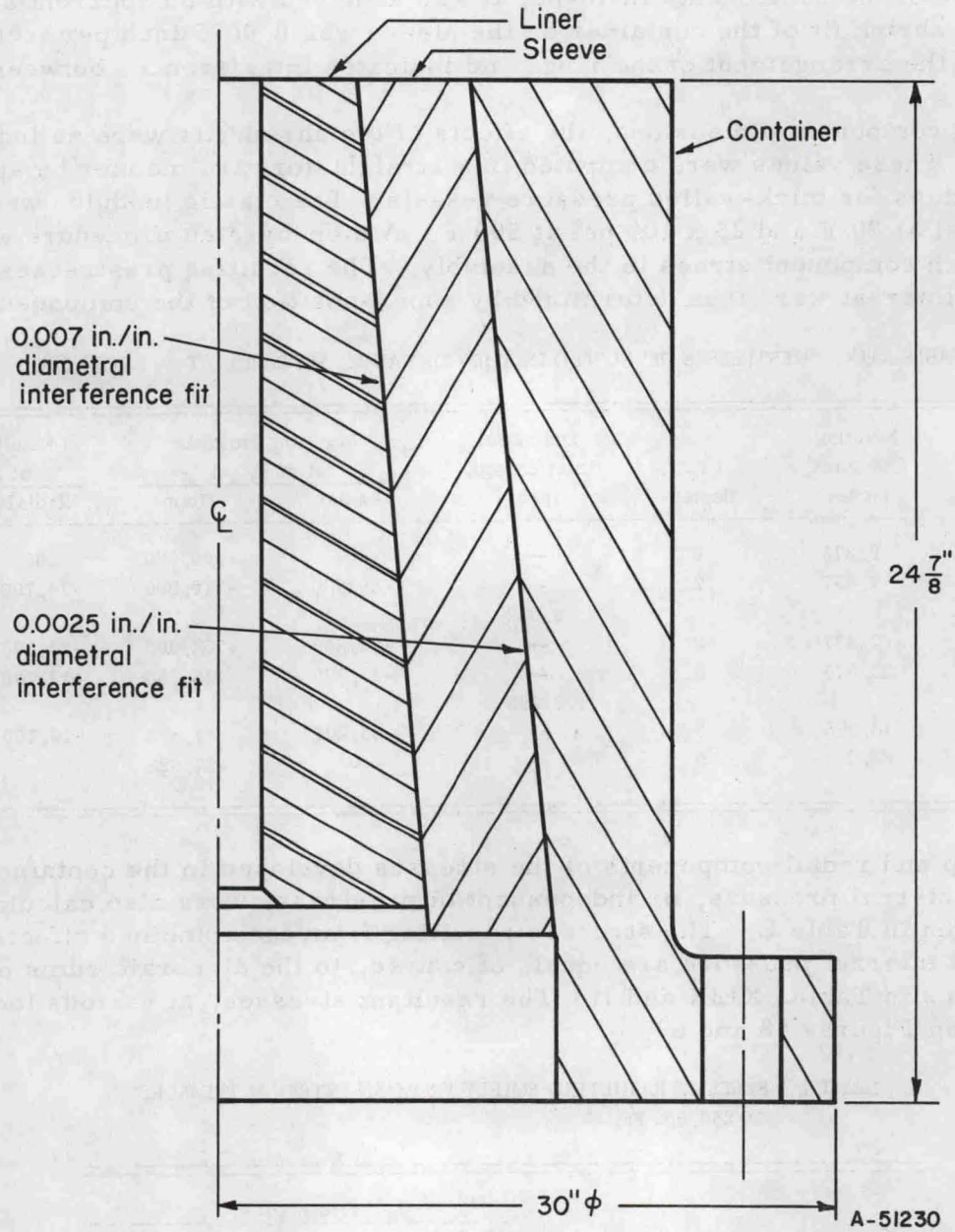

FIGURE 67. CROSS-SECTIONAL VIEW OF CONTAINER I

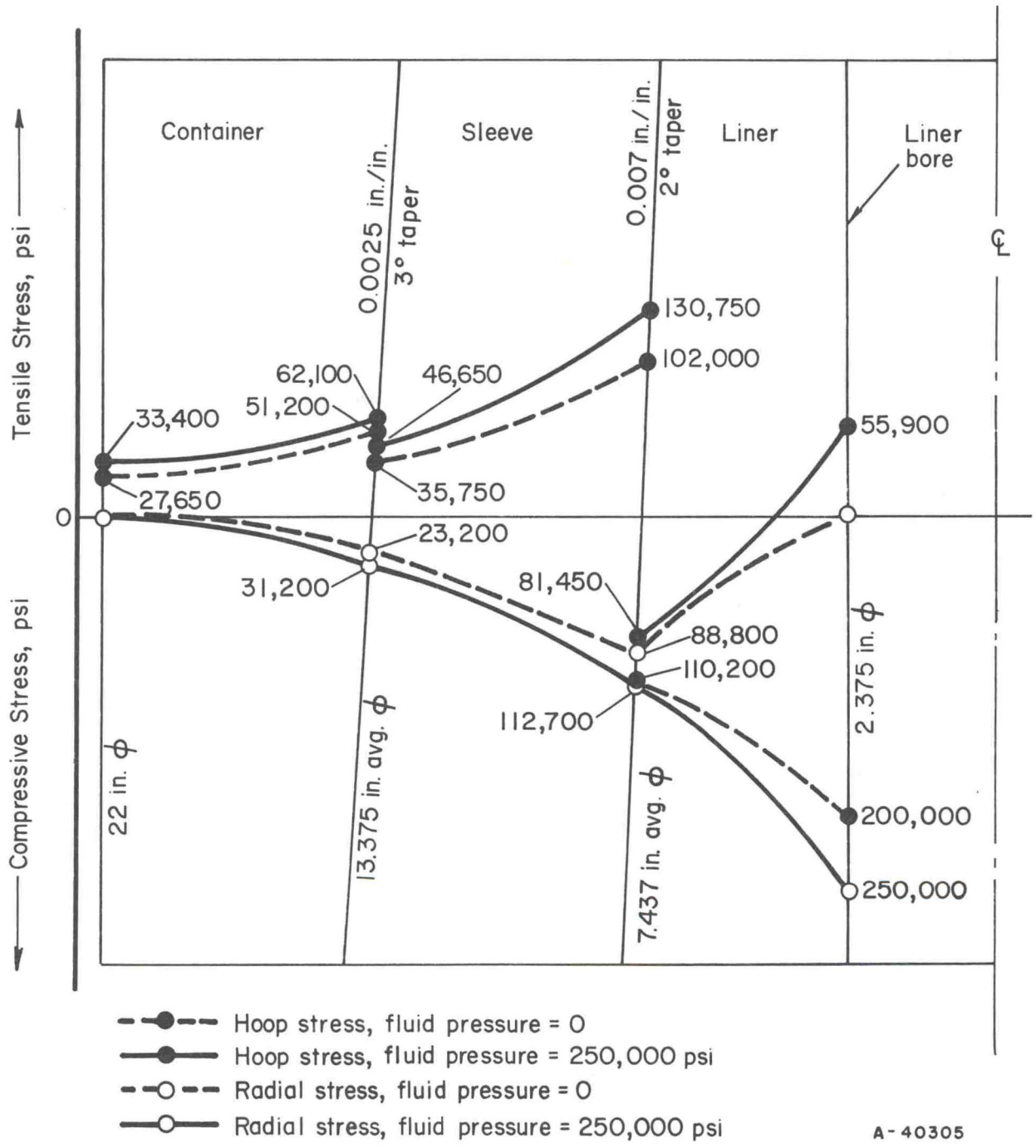

FIGURE 68. STRESS PATTERN IN CONTAINER I AT ROOM TEMPERATURE

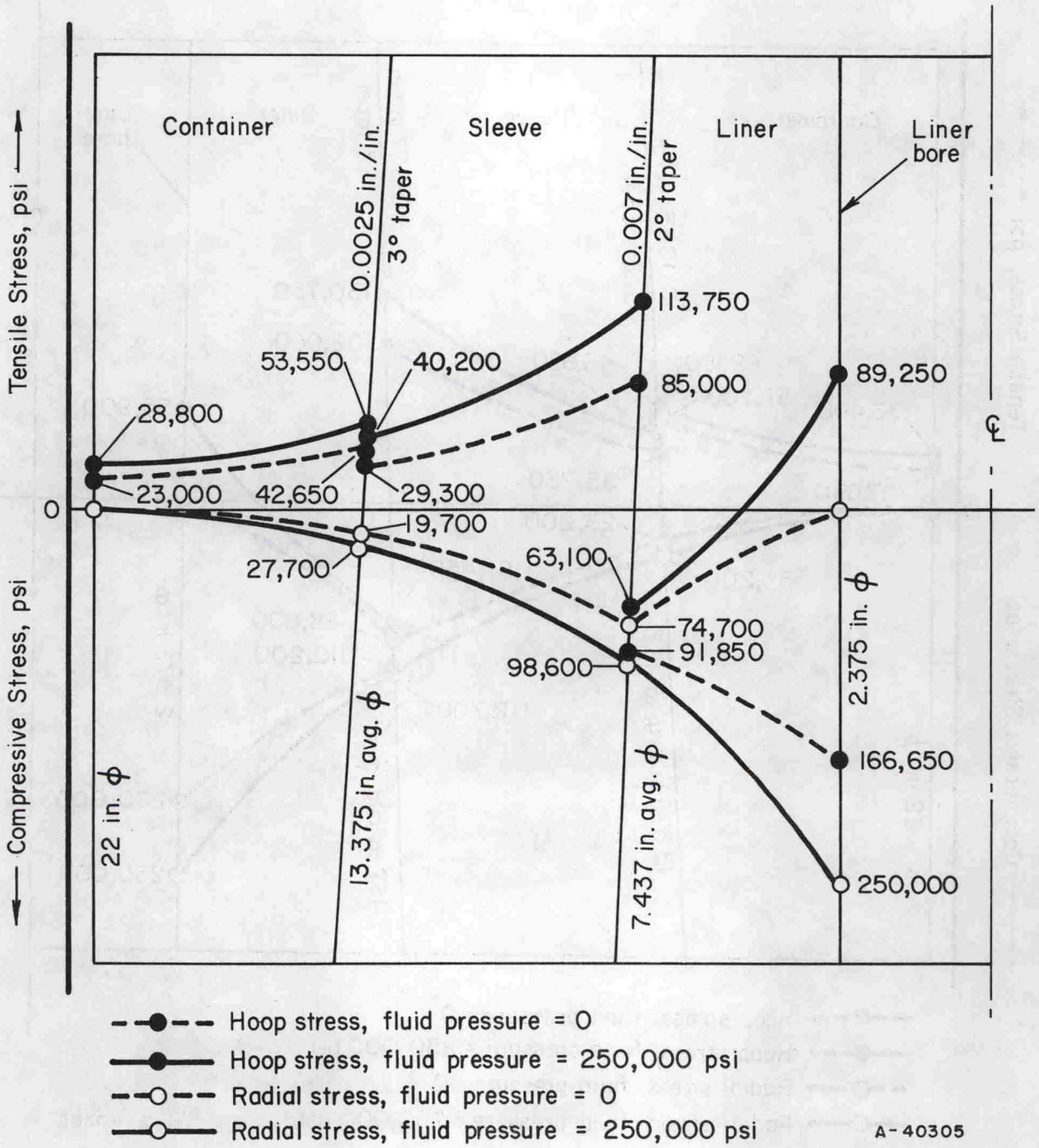

FIGURE 69. STRESS PATTERN IN CONTAINER I AT 500 F

The fact that the elastic modulus of the liner, sleeve, and container materials would be less at 500 F than at 80 F, lower estimates of interfacial pressures and prestresses were obtained.

The combined effect of the liner-sleeve and sleeve-container shrink fits caused a hoop prestress of -200,000 psi, at 80 F, on the liner bore. Figure 68 shows that, for this amount of precompression, an internal pressure of 250,000 psi produces a tensile hoop stress on the bore of only 55,900 psi. As shown in Figure 69, a similar internal pressure at 500 F would produce a tensile hoop stress of 89,250 psi at the bore.

In spite of these relatively low hoop stresses, obtained by using the heavy shrink fits, the effective stresses at the bore are extremely severe. For example, the effective shear stress at 500 F, where σ_1 = +89,250 psi and σ_3 = -250,000 psi, is approximately 175,500 psi. This means that the uniaxial yield strength of the liner material at 500 F would have to be about 304,000 psi to avoid yielding. Obviously, this is a difficult requirement for most liner materials to meet.

The types of steel ordinarily used for hot-working tools do not have sufficient strength for the application. Some of the high-speed-type tool steels which will develop adequate strength levels are lacking in ductility. Although tungsten carbide has an extremely high compressive strength, the cost of such a large component would be prohibitive.

The compositions of the steels selected for the three parts of the container assembly are given in Table LI. The steel selected for the liner appeared to have the most suitable combination of strength and ductility of materials available in suitable sections. It was less expensive than some of the other materials considered such as tungsten carbide. Both the liner and sleeve were made from steel produced by consumable-electrode vacuum-melting practices. It was expected that this melting process would minimize alloy segregation and inclusion contents. The heat treatments given the components, and the resulting hardnesses, are also given in Table LI.

The components were subjected to ultrasonic inspection at different stages of manufacture. One forging intended for the container ring was scrapped in the rough-machined condition on the basis of the inspection.

The mating surfaces of the components were finished to a surface roughness of 65 μ-in., rms. The inside surface of the liner was ground to a surface finish of 4 μ-in., rms. The smoother surface minimizes the possibility of fluid leaking past the seals at high pressures.

Operational Capabilities Predicted by Theory

Despite the high stresses on the liner and sleeve, stress analyses indicated that the container assembly would meet or closely approach the operational requirements. Table LII presents the results of the stress analyses of greatest interest. The safety factors listed were based on reasonable estimates of the tensile yield strengths and the effective stresses computed by the Hencky-Von Mises relationship. They indicated the container assembly was capable of operating at an internal pressure up to 250,000 psi at room temperature and up to 230,000 psi at 500 F.

TABLE LI. COMPOSITIONS, HEAT TREATMENTS, AND HARDNESSES OF THE COMPONENTS USED FOR CONTAINER I

	Liner AISI M50	Sleeve AISI H11	Container AISI 4340
Composition, percent			
Carbon	0.80	0.41	0.35
Chromium	3.96	5.10	0.97
Molybdenum	4.05	1.23	0.41
Vanadium	1.10	0.50	0.11
Nickel	0.06	--	2.49
Manganese	0.23	0.27	0.70
Silicon	0.20	0.94	0.28
Phosphorus	0.01	0.002	0.012
Sulfur	0.007	0.003	0.011
Cobalt	0.02	--	--
Copper	0.06	--	--
Tungsten	0.03	--	--
Heat Treatment			
Preheat	1500 F for 1-1/2 hours		
Austenitize	2000 F for 1/4 hour	1850 F for 1-1/2 hours	1570 F for 6 hours
Quench	1050 F for 5 min. in salt bath, air cool	Air cool	Oil bath
Temper	1000 F for 6 hours 1000 F for 6 hours	1000 F for 4 hours 1025 F for 4 hours 1025 F for 4 hours	900 F for 12 hours
Hardness			
Rockwell "C"	63	57/58	43

TABLE LII. SAFETY FACTORS ESTIMATED FOR THE COMPONENTS OF CONTAINER I FOR VARIOUS OPERATING CONDITIONS

Component	Type of Steel	Tensile Temperature, F	Tensile Yield Strength(a), psi	Shear Yield Strength(b), psi	Internal Pressure, psi	Effective Stress on Component(c), psi	Safety Factor(d)
Liner (ID)	AISI M50	80	330,000	190,000	250,000	162,250	1.17
		500	290,000	167,000	250,000	173,500	0.95
		80	330,000	190,000	230,000	144,000	1.32
		500	290,000	167,000	230,000	156,500	1.07
Sleeve (ID)	AISI H11	80	240,000	138,500	250,000	121,000	1.14
		500	215,000	124,000	250,000	106,250	1.17
		80	240,000	138,500	230,000	117,000	1.18
		500	215,000	124,000	230,000	104,250	1.19
Container (ID)	AISI 4340	80	160,000	92,300	250,000	47,250	1.95
		500	125,000	72,100	250,000	41,250	1.75
		500	125,000	72,100	230,000	40,750	1.77

(a) Estimated from measured hardnesses.

(b) Estimated as being 0.577 of tensile yield strength.

(c) Stress computed by Hencky-Von Mises relationship; shear stress by Tresca relationship would be approximately 2 to 6 percent lower.

(d) Based on ratio of shear yield strength to effective stress.

During the experimental research program the container assembly was operated approximately 12 times at 500 F and pressures up to 250,000 psi on the ram or stem. Based on experience at room temperature, the internal fluid pressures in those experiments are believed to have reached about 225,000 psi at the inside surface of the liner. The container was operated in approximately 350 experiments at room temperature. Fluid pressures inside the container ranged up to 265,000 psi. However, early in this program, the liner failed after holding at a fluid pressure of 246,000 psi (at 80 F) for 2-3/4 minutes. The failure consisted of a longitudinal crack that ran from the bottom of the liner to about 3-1/2 inches from the top and terminated in a transverse crack. At the time of failure, the stem was inserted about 4 inches into the liner bore. The longitudinal crack did not extend much beyond this point, evidently because of the high compressive prestresses on the bore above the stem seals.

The liner had been made from consumable, vacuum-melted AISI-M50 tool steel. Examination of the fractured surfaces of the liner by several techniques indicates that the failure resulted from low-cycle fatigue. The failure appears to have initiated at a point near the middle of the longitudinal crack. A photomacrograph at 25X of the fractured surface at the suspected point of initiation is shown in Figure 70. It is noted that radial markings appear to emanate from a small round void indicated by an arrow. This void is approximately 0.005 inch in diameter and is located about 0.008 inch beneath the liner bore surface. The mating fractured surface contains a protrusion which appears to match the void in size, shape, and location.

The precise nature of the protrusion is not known. It is suspected that it is an inclusion, although it is unusually large for consumable, vacuum-melted materials in which inclusions generally are no larger than about 0.0005 inch. This was found to be

25X 25674

FIGURE 70. FRACTOGRAPH OF FRACTURED SURFACE OF LINER OF CONTAINER I

Arrow points to void located about 0. 008 inch beneath the linet bore surface.

the case on metallographic examination of other specimens taken close to the origin of failure. In spite of the relatively large size of the suspected defect, however, it is still far below the sensitivity range (3/64 inch) of the ultrasonic equipment used to inspect the liner during fabrication. Detection would have been made even more difficult, of course, if the protrusion had filled the void completely at the time of testing.

Electron microscopic fractography was employed to determine the mode of crack propagation in the vicinity of the origin. A standard two-stage plastic carbon replication technique was used to obtain replicas of an area approximately 0.1 inch^2 containing the above described void. Examination at a magnification of 12,200X revealed the fractured surface to be generally flat and featureless with localized regions containing very fine fatigue striations. The fatigue striations are indicated by the arrows in the electron microscopic fractograph shown in Figure 71. The small spacing of the striations suggests that crack growth may not have been due to the extrusion pressure cycles alone, but also to a vibration or pulsation superimposed on the high pressure. An obvious source of this vibration is the hydraulic pump of the press which can transmit pulsations to the liner by way of the stem and hydrostatic fluid. The extent to which such vibrations may have contributed to the rate of crack growth is not known.

Another feature of significance is evident in the fractograph shown in Figure 72. This is the typical cleavage-type fracture (fan-like striations indicated by arrow) of undissolved carbides. This observation indicates that these particles would have accelerated growth of the fatigue crack by fracturing in a brittle manner on a single cycle of load over a distance much larger than the crack growth per cycle indicated by the very fine striations noted earlier.

Metallographic examination of an area adjacent to the void revealed interdendritic networks of undissolved carbide particles.

Container II

Revised Container-Assembly Design

Tooling components that are made from low-ductility materials and operate in service at low safety factors are prone to failure by low-cycle fatigue.[23, 48] The liner component is a case in point. To minimize possible problems with low-cycle fatigue, it was felt at the time that the service stresses should be held below the elastic limit, rather than below the 0.2 percent offset yield strength of the material. One of the problems, however, was the lack of adequate and reliable data on elastic limit and yield strength of AISI-M50 steel (liner material) in the hardness range of R_C 61 to 63. In the absence of such data, a minimum safety factor of 1.25 (based on best estimates of yield strength) was selected for the revised design to reduce the possibility of stressing the component above the elastic limit.

Changes in the container assembly design aimed at increasing the safety factor were necessarily limited to those which would keep fabrication costs to a minimum. Thus, possible design changes were narrowed to two options, both of which included use of the present sleeve and container components. In one design, use of a tungsten carbide liner was considered because of its high compressive yield strength. However, this design was eliminated because the difference in thermal-expansion coefficients between steel and carbide (6.5×10^{-6} versus 2.5×10^{-6} inch/inch/F) would cause the

12,200X E1646A

FIGURE 71. ELECTRON MICROSCOPIC FRACTOGRAPH SHOWING FINE FATIGUE STRIATIONS IN LINER OF CONTAINER I

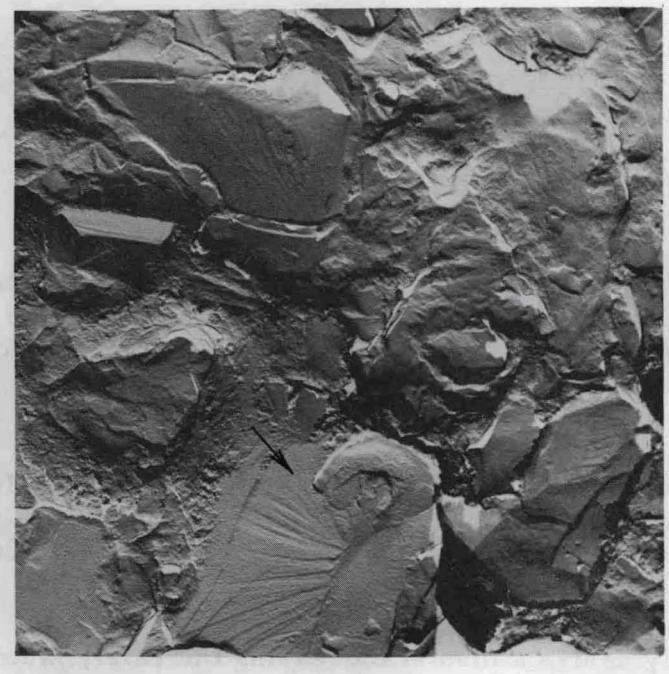

6,200X E1646E

FIGURE 72. ELECTRON MICROSCOPIC FRACTOGRAPH SHOWING CLEAVAGE FRACTURE OF UNDISSOLVED CARBIDES IN LINER OF CONTAINER I

required interference fit between the liner and sleeve to be lost during operation at 500 F.

The second design consisted of replacing the liner component with two rings which occupy the same volume as did the liner component. This design was used because calculations indicated that the safety factor could be increased to a minimum of about 1.25 without resorting to any larger interference fits than were used in the present container assembly.

The final revised container assembly design is illustrated in Figure 73. To avoid possible confusion, the designations for the component rings have been changed as follows:

Container I (Figure 67)	Container II (Figure 73)
Liner	Liner
(None)	Sleeve 1
Sleeve	Sleeve 2
Container	Container

In other words, Sleeve 1 was a new addition to the old design, but Sleeve 2 is the same component as the "sleeve" in the old design.

Stress Analysis

Referring to Figure 73, it can be seen that the liner was assembled with the same manufactured* interference fit of 0.007 in./in. as that in the previous container. However, because the liner in Container II had a thinner wall such an interference would generate a higher hoop prestress on assembly than was obtained in Container I providing the "assembly" interferences were also of the same order. To achieve the same "assembly" interference between the liner and Sleeve 1 shown in Figure 73 as that obtained in Container I, it was found necessary to manufacture an interference of 0.0048 in./in. between Sleeve 1 and Sleeve 2. Measurements of the liner bore before and after assembly were used to determine the actual stress distribution achieved in the assembly. Equations 13 and 14 in Section 3 were used in these calculations.

The stress patterns calculated for both room temperature and 500 F are presented in Figures 74 and 75. Each figure shows both the hoop and radial stresses developed at the ring interfaces under internal fluid pressures of 0 and 250,000 psi.

The combined interference fits of 0.0071 and 0.0048 inch per inch on the Sleeve 1-liner and Sleeve 2-Sleeve 1 interfaces, respectively, place the liner bore in precompression with a stress of 260,650 psi at room temperature. With this amount of precompression, it can be seen in Figure 4-8 that an internal pressure of 250,000 psi at room temperature produces a tensile hoop stress on the liner bore of only 5,600 psi. At 500 F, the precompression is reduced from 260,650 to 217,250 psi (Figure 75) because of the decrease in elastic moduli of the rings at this temperature. In this case, the tensile stress on the liner bore at maximum internal pressure is increased from 5,600 to 49,000 psi.

*The "manufactured" interference is that which is obtained before assembly and represents the difference in size between each mating diameter. The "assembled" interference is greater than the "manufactured" interference before assembly by an amount proportional to the extent that each ring changes dimensions elastically as the rings are assembled.

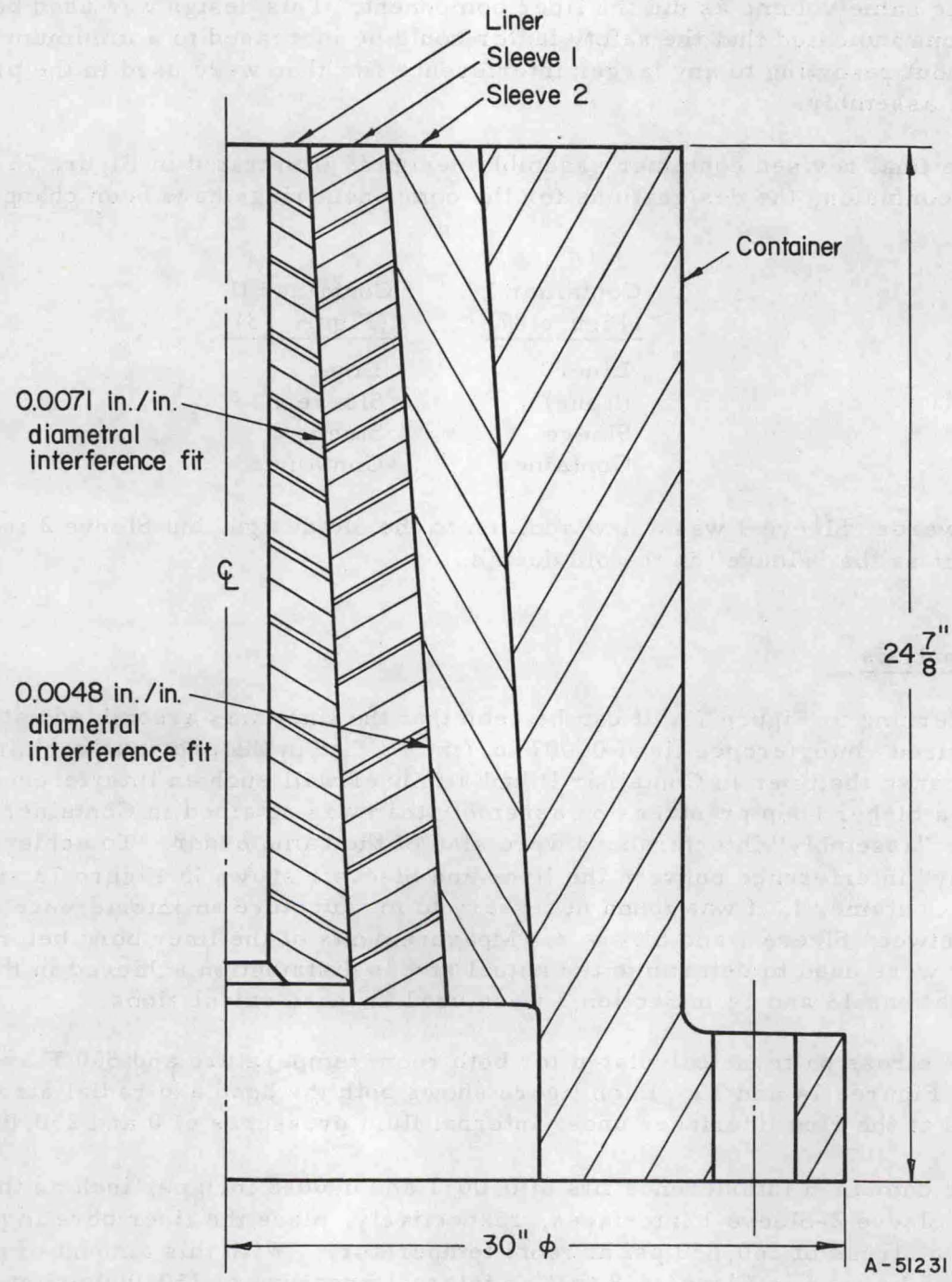

FIGURE 73. CROSS-SECTIONAL VIEW OF CONTAINER II

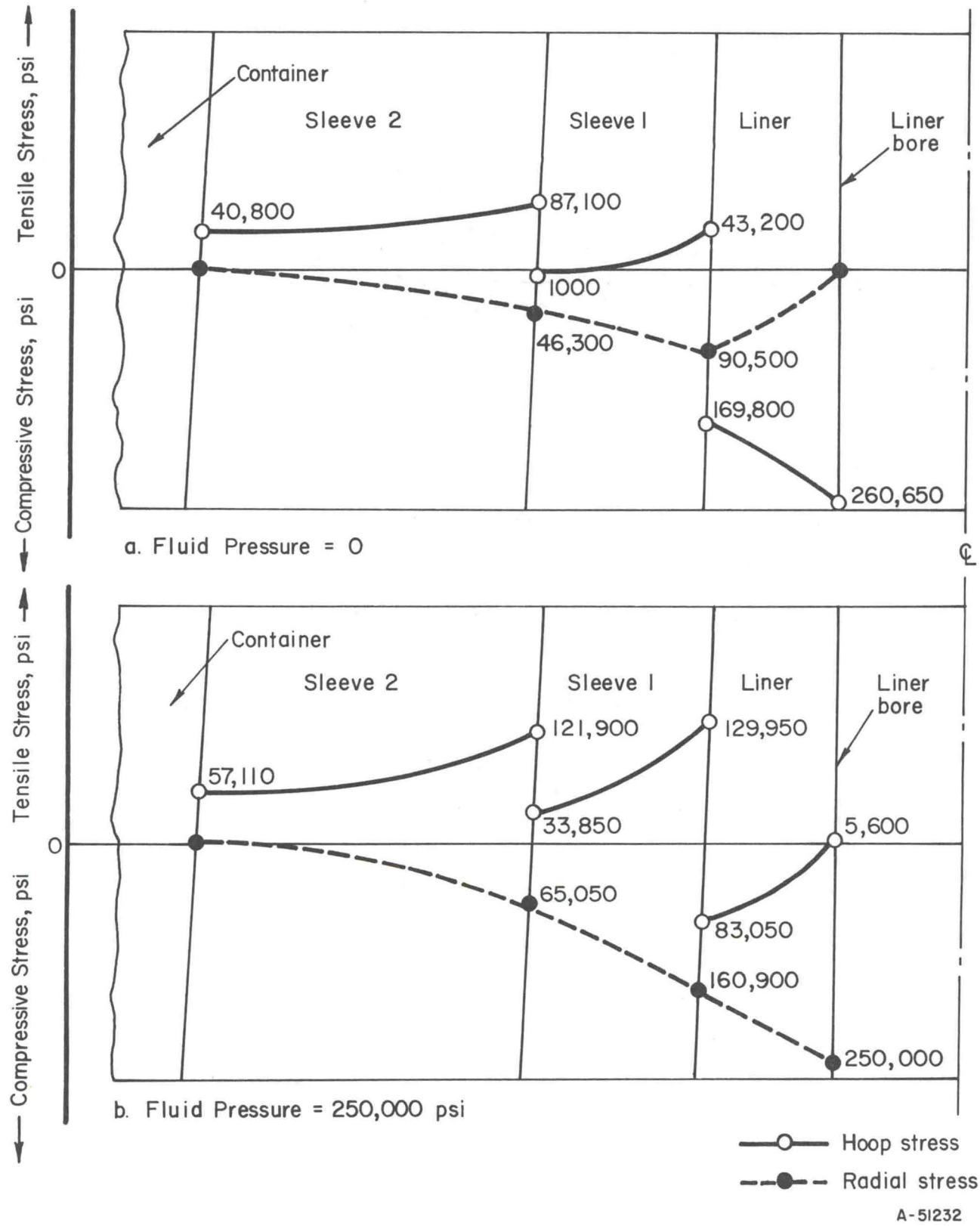

FIGURE 74. STRESS PATTERN IN CONTAINER II AT ROOM TEMPERATURE

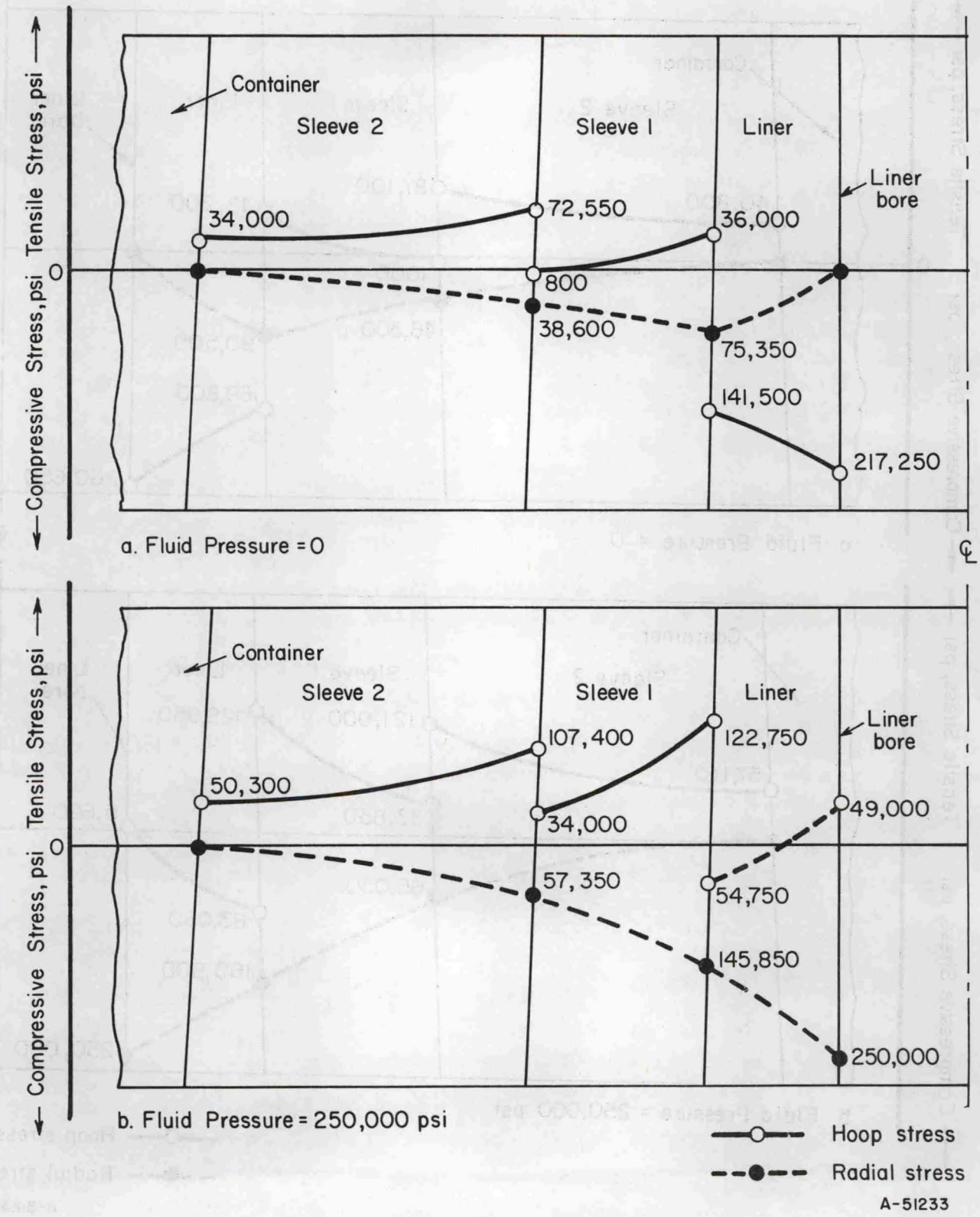

FIGURE 75. STRESS PATTERN IN CONTAINER II AT 500 F

Component Ring Materials

Consumable-electrode vacuum-melted AISI-M50 tool steel was selected for the liner and Sleeve 1 rings. This tool steel, which had been used in the original liner, was selected over other candidate steels (such as AISI-M1 or M10) because it possessed the most suitable combination of strength and ductility. Each component was hardened to R_C 61 to 63.

Sleeve 2 and the container ring were made of AISI-H11 (R_C 57) and 4340 (R_C 43) steels, respectively.

Operational Capabilities

Safety factors were calculated for internal fluid pressures of 250,000 and 230,000 psi at both room temperature and 500 F. They were also calculated for a fluid pressure of 220,000 psi at 500 F. The results of the calculations are given in Table LIII. It can be seen that the safety factors for the liner and Sleeve 1 are 1.29 and 1.30, respectively, for operation at fluid pressures of 250,000 psi at room temperature. At 500 F, the safety factors fall below the minimum of 1.25. Thus, the fluid pressure must be reduced for 500 F operation to minimize the possibility of low-cycle fatigue. At 230,000 psi, the safety factor for Sleeve 1 is 1.37 but only 1.18 for the liner. In view of this, it is recommended that fluid pressures at 500 F do not exceed about 220,000 psi. At this pressure level, the safety factors are 1.27 for the liner and 1.33 for Sleeve 1.

TABLE LIII. SAFETY FACTORS ESTIMATED FOR LINER, SLEEVE 1 AND SLEEVE 2 OF CONTAINER II FOR VARIOUS OPERATING CONDITIONS

Component	Type of Steel	Tensile Temperature, F	Tensile Yield Strength, psi	Shear Yield Strength[a], psi	Internal Pressure, psi	Effective Stress on Component[b], psi	Safety Factor[c]
Liner (ID)	AISI-M50	80	330,000	190,000	250,000	146,250	1.29
		500	290,000	167,000	250,000	160,500	1.04
		80	330,000	190,000	230,000	137,000	1.48
		500	290,000	167,000	230,000	141,500	1.18
		500	290,000	167,000	220,000	132,250	1.27
Sleeve 1 (ID)	AISI-M50	80	330,000	190,000	250,000	145,500	1.30
		500	290,000	167,000	250,000	134,500	1.24
		80	330,000	196,000	230,000	135,000	1.49
		500	290,000	167,000	230,000	128,000	1.31
		500	290,000	167,000	220,000	130,000	1.29
Sleeve 2 (ID)	AISI-H11	80	240,000	138,500	250,000	95,000	1.46
		500	215,000	124,000	250,000	83,500	1.48
		500	215,000	124,000	230,000	81,500	1.52

(a) Estimated as being 0.577 of tensile yield strength.
(b) Stress computed by Hencky-Von Mises relationship.
(c) Based on ratio of shear yield strength to effective stress.

It should be noted that the stress analysis of the revised container assembly does not include any supporting contribution from the container component. This assumption was used because it is not known whether the original interference-fit of 0.0025 inch per inch between the container and Sleeve 2 could be maintained while removing and replacing the failed liner. Therefore, the stress analysis assumed that only a metal-to-metal fit existed at this interface and that the container ring was not a load-bearing component. However, if any interference-fit did exist and the container ring did bear a portion of the load, the safety factors of the revised container assembly would be slightly higher than those shown in Table LIII.

Container III

As a result of the liner fatigue failure in Container I, it was considered desirable to have a standby container which would ensure continuity in hydrostatic-extrusion research if further failures occurred. At the same time, construction of such a container presented a unique opportunity to use the up-to-date stress analysis and design for a four-ring unit based on a fatigue-life criterion.

The Design of Container III

It was decided to construct Container III with materials whose fatigue properties were known. On the basis of the data given in Tables XLI, XLII and XLIII, AISI H11 tool steel was considered to be a good candidate material. Calculations showed that a fatigue life of 10^5 - 10^6 cycles could be achieved with AISI H11 within the 250,000 psi pressure limit.

A four-ring container, similar in dimensions to those of Container II, Figure 67, was chosen for analysis. The liner was considered to be of high-strength steel surrounded by lower strength, ductile outer rings. The analysis of residual stresses (prestresses) and the required shrink-fit interferences were programmed for calculation of the Battelle computer. The computer codes developed at Battelle for this container design were:

PROGRAM COMPHS1 - Calculation of maximum pressure-to-strength ratio for container having an ultrahigh-strength liner.

PROGRAM COMPHS2 - Calculation of operating stresses, prestresses at operating temperature, and interferences required for shrink fit assembly.

The hoop and radial components of the design prestresses and operating stresses at room temperature are plotted at their various locations in the assembly in Figure 76. The combined effect of the multiple shrink fits was to cause a compressive hoop stress of 256,000 psi on liner bore. Under an internal fluid pressure of 250,000 psi the figure shows that the design tensile hoop stress produced on the bore is zero.

The high interface and hoop stresses, bore pressures of both zero and 250,000 psi, were considered to be out of the realm of the capabilities of an alloy such as AISI 4340, which was used previously as an outer ring material. Consequently, AISI H11 tool steel in a softer condition than the liner, was chosen for the outer rings. The composition, heat treatment and hardnesses of the H11 steel produced by consumable-

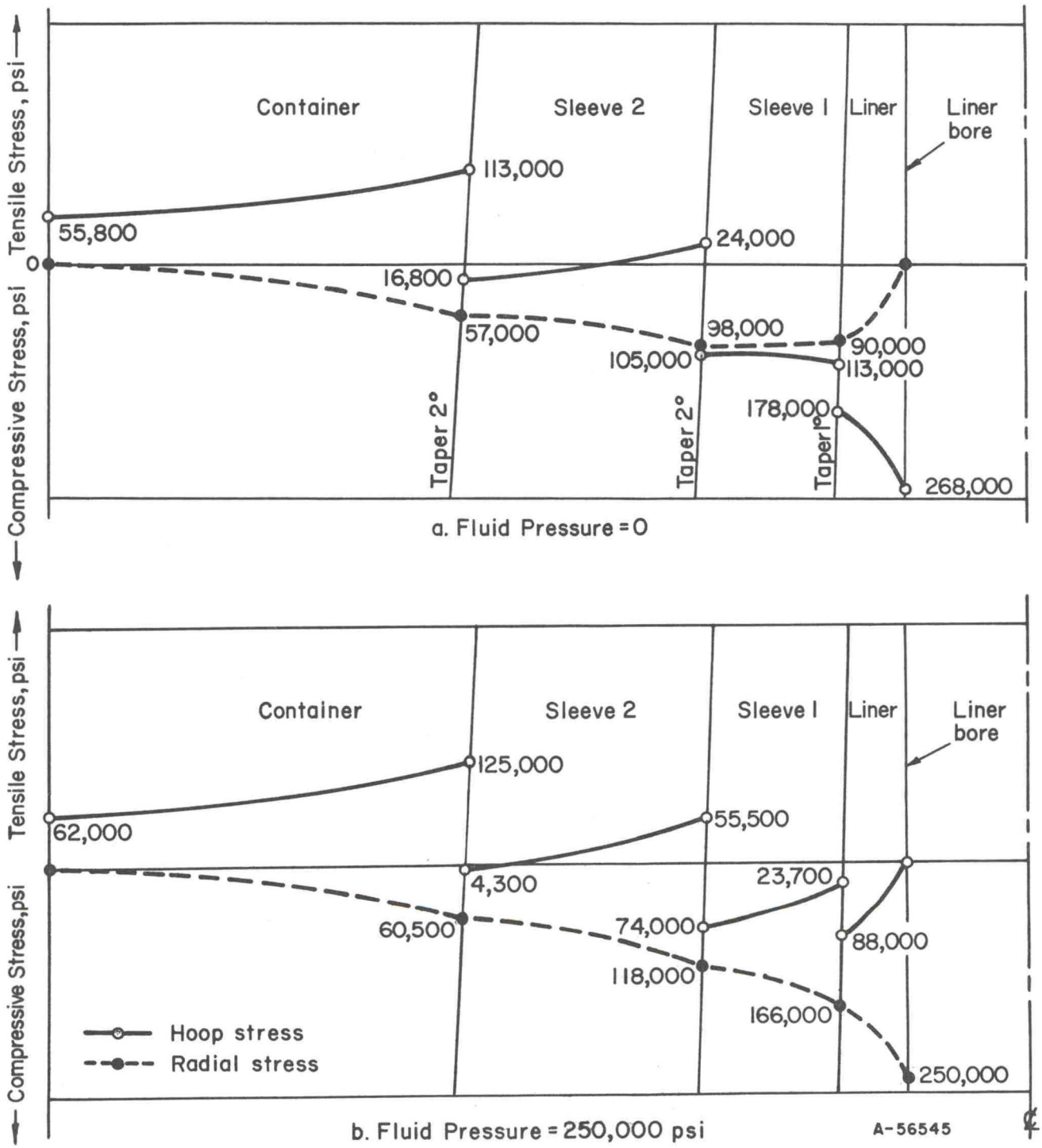

FIGURE 76. DESIGN STRESS PATTERN IN CONTAINER III AT ROOM TEMPERATURE

electrode vacuum-melting practices, used for constructing the container are given in Table LIV. A thorough ultrasonic inspection of each ring revealed no measurable defects.

TABLE LIV. COMPOSITION, HEAT TREATMENT, AND HARDNESSES OF THE COMPONENTS USED FOR THE FOUR-RING ASSEMBLY OF CONTAINER III

AISI-H11, Nominal Composition, percent - (All rings)		
0.41 Carbon	5.1 Chromium	1.23 Molybdenum
0.5 Vanadium	0.27 Manganese	1.0 Silicon

Heat Treatment			
Austenitize	1850 F for 1-1/2 hr	All rings	
Quench	Air cool		
Temper, liner	950 for 2 hr		
	1000 for 2 hr		
	1000 for 2 hr		Hardness - R_C 54/56
Temper, outer three rings	1090 for 4 hr		
	1100 for 4 hr		
	1110 for 4 hr		Hardness - R_C 44/46

Because the whole container unit was made from the same material, the coefficient of thermal expansion in each ring under temperature was the same. (It was not expected that differences in hardness levels of the rings would markedly affect the coefficient of thermal expansion.) Therefore, the stress distribution pattern for the rings at 500 F would be the same as those shown in Figure 76b. However, the pressure capability at 500 F is limited to 225,000 psi by the effect of temperature on strength. Therefore, the interface stresses predicted in Figure 76b would be less proportionately to the bore stresses, in service at 500 F. The same pressure limit, 225,000 psi at 500 F was also imposed on Containers I and II.

It is pertinent at this stage to compare the residual stress patterns in Container II, Figure 74a, with those predicted for Container III. It is seen that the design hoop prestress of 268,000 psi in the H-11 liner of Container III is about 3 percent higher than that for the harder AISI-M50 liner in Container II. In view of the lack of knowledge of the fatigue properties of AISI-M50 it is not possible to determine what the predicted fatigue life of Container II would be. However, rotating-beam fatigue data obtained on a similar type of material AISI M2 at a hardness of R_C 62, suggests that the fatigue limit at 10^6 cycles for AISI-M50 might be about 140,000 psi whereas for AISI H11 the corresponding figure is 150,000 psi.[49]

Container Assembly

The four rings, which were slightly tapered for press fitting, were assembled by a hydraulic press from the outer ring inwards. A lubricant was applied to the interfaces of the rings to ease assembly. The calculated press loads required for assembly

are given below with the associated manufactured interferences. The press loads were estimated by assuming an interface coefficient of friction of 0.1.

Ring	Load, tons	Manufactured Interference, inch/inch
Sleeve 2 into container housing	1500	0.00208
Sleeve 1 into assembly	1040	0.00443
Liner into assembly	1130	0.00443

It is important to note that all the interferences given above are as manufactured and not as generated during assembly. The assembly interference achieved in pressing the liner into position was 0.0092 inch/inch. It was not possible to determine the actual press loads required because in each case, the rings were pressed home in a continuous stroke up to the press capacity of 2200 tons.

By measuring the liner bore diameter before and after its assembly, the actual surface hoop prestress was calculated to be -255,000 psi. This is lower than the design prestress of -268,000 psi. While the maximum pressure capability of the container remains at 250,000 psi, the effect of the reduction in prestress obtained is expected to marginally reduce the fatigue life (10^6 cycles) compared to the design value.

APPENDIX I

ELASTICITY SOLUTION FOR A RING SEGMENT

A ring segment is shown in Figure 77. Its geometry is defined by the radii r_1 and r_2 and the angle α. The loading of the segment is a pressure p_1 at r_1 and p_2 at r_2. For equilibrium, p_2 is related to p_1 by Equation (21) in the text; i.e.,

$$p_2 = \frac{p_1}{k_2} \tag{92}$$

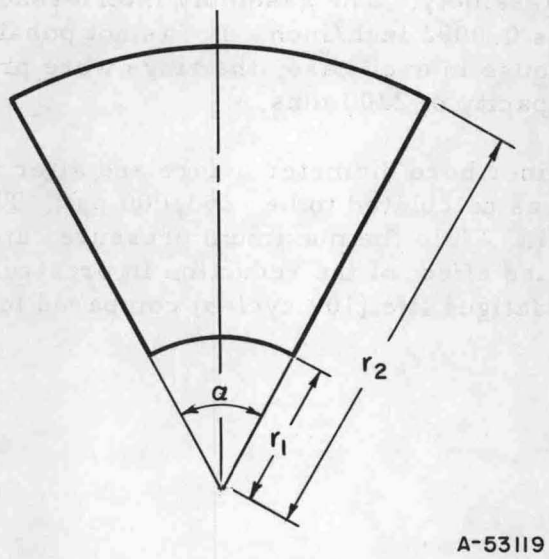

FIGURE 77. GEOMETRY OF RING SEGMENT

The solution for the stresses within the segment is found by superposition of two solutions: The Lamé solution for a cylinder, Equations (13a-c) and (14a, b) in the text, plus a bending solution, Equations (48) and (53) in Reference (41). The bending solution removes the moment from the sides of the segment that exists in the Lamé solution. The latter equations for the bending solution are written as

$$(\sigma_r)_b = \frac{4M_1 p_1}{\beta_1} f_1(r), \quad (\sigma_\theta)_b = \frac{4M_1 p_1}{\beta_1} f_2(r), \quad (\tau_{r\theta})_b = 0 \tag{93a-c}$$

and

$$\left(\frac{u}{r}\right)_b = \frac{M_1 p_1}{E_2 \beta_1} f_3(r) + \frac{G_1 p_1}{r} \cos\theta$$

$$\left(\frac{v}{r}\right)_b = \frac{8M_1 p_1}{E_2 \beta_1} (k_2^2 - 1)\,\theta - \frac{G_1 p_1}{r} \sin\theta \qquad (94a\text{-}c)$$

where $f_1(r)$, $f_2(r)$, and $f_3(r)$ are defined by Equations (20a-c) in the text and where

$$\beta_1 \equiv (k_2^2 - 1)^2 - 4k_2^2 (\log k_2)^2 \qquad (95)$$

The moment $M = M_1 p_1 r_1^2$ is found by integrating the negative of the Lamé hoop stress $(\sigma_\theta)_c$ for a cylinder given by Equation (13b) in the text over the side of the segment; i.e.,

$$M = -\int_{r_1}^{r_2} (\sigma_\theta)_c \, r \, dr \ ,$$

hence,

$$M_1 = \frac{-1}{p_1 r_1^2} \int_{r_1}^{r_2} \left\{ \frac{(p_1 - p_2 k_2^2)}{k_2^2 - 1} - \frac{(p_2 - p_1) k_2^2}{k_2^2 - 1} \left(\frac{r_1}{r}\right)^2 \right\} r \, dr$$

$$M_1 = -\frac{1}{2}\left(1 - \frac{p_2}{p_1} k_2^2\right) + \left(\frac{p_2}{p_1} - 1\right) \frac{k_2^2}{k_2^2 - 1} \log k_2 \qquad (96)$$

G_1 is found by taking a reference point for the radial deflection u. If the point $r_0 = \frac{r_1 + r_2}{2}$, $\theta = 0$ is fixed,

then

$$G_1 = -\frac{M_1 r_0}{E_2 \beta_1} \left\{ -4(1+\nu) k_2^2 \left(\frac{r_1}{r_0}\right)^2 \log k_2 + 4(1-\nu) \left[k_2^2 \log\left(\frac{r_0}{r_1}\right) - \log \frac{r_0}{r_1} \right] - 4(k_2^2 - 1) \right\} \qquad (97)$$

The equations for the total stresses and displacements in ring segments were programmed on the computer and some calculations carried out. Example results are given in Table LV for $k_2 = 2.0$ and $\alpha = 60$ degrees. It is noted that a small residual stress σ_θ remains on the side of the segments. To be more accurate, i.e., to achieve sides entirely free of stress, the residual σ_θ could be removed by using a "dipole" solution in addition to the bending solution. However, the self-equilibrating residual stress that would be removed has a local edge effect according to the principle of St. Venant. Therefore, the σ_θ stresses in Table LVI are believed to be indicative of the actual magnitude of hoop stresses in segments at the center.

TABLE LV. STRESSES AND DEFLECTIONS IN A RING SEGMENT, $k_2 = 2.0$, $\alpha = 60°$, $\nu = 0.3$

r/r_1	σ_r/p_1	σ_θ/p_1	$\frac{Eu}{rp_1}$ at $\theta = 0°$	$\frac{Ev}{rp_1}$ at $\theta = 30°$
1.0	-1.0000	0.0394	0.6324	-0.1301
1.1	-0.9068	0.0123	0.4877	-0.0853
1.2	-0.8310	-0.0033	0.3747	-0.0480
1.3	-0.7676	-0.0112	0.2846	-0.0164
1.4	-0.7137	-0.0137	0.2117	0.0107
1.5	-0.6670	-0.0126	0.1519	0.0341
1.6	-0.6260	-0.0089	0.1022	0.0547
1.7	-0.5896	-0.0033	0.0606	0.0728
1.8	-0.5568	0.0035	0.0254	0.0890
1.9	-0.5271	0.0113	-0.0046	0.1034
2.0	-0.5000	0.0197	-0.0303	0.1163

Appreciable bending, displacement v, is also noted. The bending increases with segment size and angle α as shown in Table LVI. This bending would tend to cause the segments to dig into the liner as shown in Figure 78. Therefore, it is recommended that segments be designed with radii larger than the radii of mating cylinders in order to compensate for the change in radii due to bending. This is illustrated in Figure 78.

Note that the deflection u in Table LV can have an arbitrary translational component; i.e., the segment is free to move radially a constant amount. In calculating interferences, the difference in deflection $u(r_1) - u(r_2)$ at $\theta = 0°$ is used and the constant amount drops out.

ELASTICITY SOLUTION FOR A PIN SEGMENT

A pin segment is shown in Figure 79. Its geometry is defined by the radii r_1 and r_2 and the angle α. r_2 is taken to the inside of the pin holes as indicated. The loading of the pin segment is more complicated than that of the ring segment as shown in Figure 80. A constant pressure p_1 is assumed to act at the inside. A variable pressure is assumed to act at the outside, i.e.,

$$\sigma_r = -p_1, \text{ at } r_1$$

$$\sigma_r = -p_2 (1 + \cos m\theta), \text{ at } r_2 \qquad (98a, b)$$

In addition, a shear acts at r_2:

$$\tau_{r\theta} = -\tau \sin m\theta, \text{ at } r_2 \qquad (98c)$$

TABLE LVI. DEFLECTIONS IN RING SEGMENTS, $\nu = 0.3$

(a) $\alpha = 60°$

k_2	$\frac{Eu}{rp_1}$ at $\theta = 0°$		$\frac{Ev}{rp_1}$ at $\theta = \alpha$	
	$r = r_1$	$r = r_2$	$r = r_1$	$r = r_2$
1.1	0.3463	0.2291	-0.0008	0.0447
1.2	0.3899	0.1730	-0.0221	0.0612
1.3	0.4287	0.1494	-0.0408	0.0652
1.4	0.4642	0.1153	-0.0576	0.0743
1.5	0.4970	0.0611	-0.0726	0.0931
2.0	0.6324	-0.0303	-0.1301	0.1163
3.0	0.8251	-0.0905	-0.2013	0.1243

(b) $k_2 = 2.0$

α	$\frac{Eu}{rp_1}$ at $\theta = 0°$		$\frac{Ev}{rp_1}$ at $\theta = \alpha/2$	
	$r = r_1$	$r = r_2$	$r = r_1$	$r = r_2$
45°	0.6324	-0.0303	-0.1052	0.0835
60°	0.6324	-0.0303	-0.1301	0.1163
90°	0.6324	-0.0303	-0.1529	0.1957

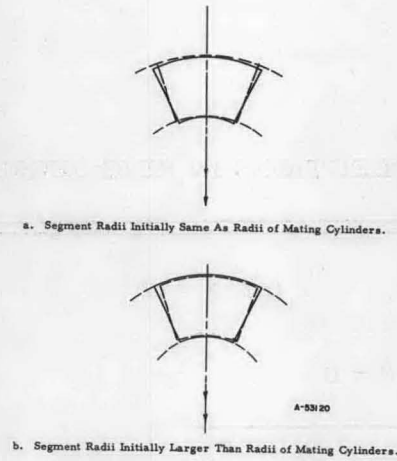

FIGURE 78. BENDING DEFORMATION OF RING SEGMENTS

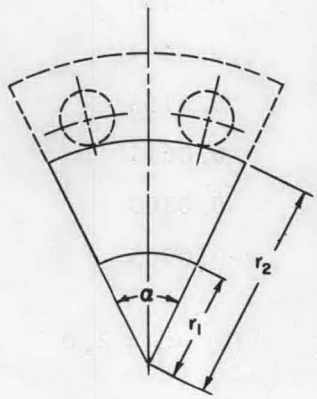

FIGURE 79. GEOMETRY OF PIN SEGMENT

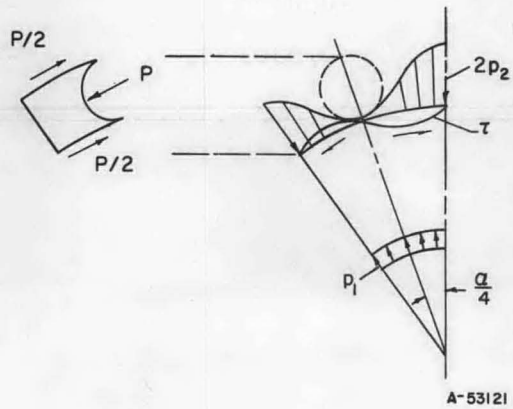

FIGURE 80. LOADING OF PIN SEGMENT

where

$$m = 4\pi/\alpha \tag{99}$$

If N_s is the number of segments then $m = 2N_s$.

The shear force $\tau_{r\theta}$ must balance the pin force P shown in Figures 80 and 81. From Figure 80, it is seen for equilibrium of P, that it is required

$$t\int_{\alpha/4}^{\alpha/2} \tau_{r\theta} \cos\left(\theta - \frac{\alpha}{4}\right) r_2 d\theta = P/2$$

where t is the segment thickness. Substitution of (98c) into this integral and integration gives

$$\tau = \frac{(m^2 - 1)\, P}{2mtr_2\,(1 + \cos \pi/m)} \tag{100}$$

where P must be in equilibrium with p_1 as shown in Figure 81, i.e.,

$$P = p_1 r_1 t \ . \tag{101}$$

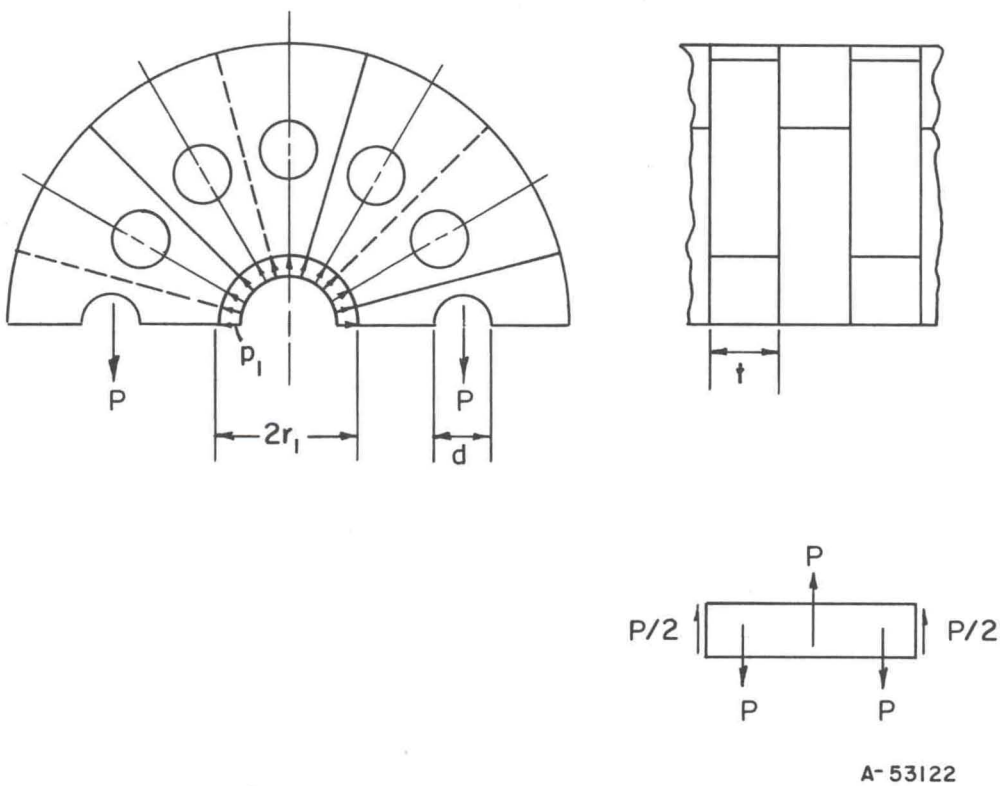

FIGURE 81. LOADING OF PINS

For radial equilibrium of the loadings shown in Figure 80, p_2 can be found by integration, i.e.,

$$2\int_0^{\alpha/2} [\tau_{r\theta}\sin\theta - \sigma_r \cos\theta]\, r_2 d\theta \Big|_{r_2} = 2p_1 r_1 \sin\frac{\alpha}{2} \quad .$$

Substitution for $\tau_{r\theta}$ and σ_r from (98b, c) and integration gives

$$p_2 = \frac{1}{(m^2-2)} \left[(m^2-1)\frac{p_1}{k_2} - m\tau\right] \quad . \tag{102}$$

The stresses in a pin segment are found by superposition of three solutions: the Lamé solution for constant pressures p_1 and p_2 at the r_1 and r_2 respectively, a sinusoidal solution for the variable σ_r loading $-p_2 \cos m\theta$ at r_2, and a bending solution to remove the hoop stress of the first two solutions from the sides of the segments. The Lamé solution is given by Equations (13a-c) and (14a, b) in the text. The sinusoidal solution, taken from the cos $m\theta$ part of Equation (81) in Timoshenko and Goodier[41], is

$$\sigma_r = \Big[m(1-m)\, a_m \rho^{m-2} + (2-m)(1+m)\, b_m \rho^m - m(m+1)\, c_m \rho^{m-2} + (2+m)(1-m)\, d_m \rho^{-m}\Big] \cos m\theta$$

$$\sigma_\theta = \Big[m(m-1)\, a_m \rho^{m-2} + (m+2)(m+1)\, b_m \rho^m + m(m+1)\, c_m \rho^{-m-2} + (m-2)(m-1)\, d_m \rho^{-m}\Big] \cos m\theta \tag{103a-c}$$

$$\tau_{r\theta} = m\Big[(m-1)\, a_m \rho^{m-2} + (m+1)\, b_m \rho^m - (m+1)\, c_m \rho^{-m-2} + (-m+1)\, d_m \rho^{-m}\Big] \sin m\theta$$

where

$$\rho \equiv r/r_2 \quad . \tag{104}$$

From the boundary conditions $\sigma_r = 0$, $\tau_{r\theta} = 0$ at r_1 and $\sigma_r = -p_2 \cos m\theta$, $\tau_{r\theta} = -\tau \sin m\theta$ at r_2 for the sinusoidal solution, the constants a_m, b_m, c_m, and d_m are found to be

$$a_m = \left(\frac{-p_2}{2} + \frac{\tau}{2}\right)\left[\frac{m^2 + (1-m^2)\, k_2^2 - k_2^{2m+2}}{\beta_2 (m-1)}\right] + \left(\frac{-p_2}{2} - \frac{\tau}{2}\right)\frac{k_2^2 (1 - k_2^{2m})}{\beta_2}$$

$$b_m = \left(\frac{-p_2}{2} + \frac{\tau}{2}\right) \frac{mk_2^2}{\beta_2} (k_2^2 - 1)$$
$$-\left(\frac{-p_2}{2} - \frac{\tau}{2}\right) \frac{m(k_2^2 - k_2^{2m+2})}{(m+1)\beta_2}$$

$$c_m = -\left(\frac{-p_2}{2} + \frac{\tau}{2}\right) \frac{k_2^2 (1 - k_2^{-2m})}{\beta_2}$$
$$+\left(\frac{-p_2}{2} - \frac{\tau}{2}\right)\left[\frac{(1 - m^2) k_2^2 - k_2^{-2m+2} + m^2}{\beta_2 (m+1)}\right] \qquad (105)$$

$$d_m = \left(\frac{-p_2}{2} + \frac{\tau}{2}\right) \frac{mk_2^2 (k_2^2 - k_2^{-2m})}{\beta_2 (m-1)}$$
$$+\left(\frac{-p_2}{2} - \frac{\tau}{2}\right) \frac{m}{\beta_2} k_2^2 (k_2^2 - 1)$$

where

$$\beta_2 \equiv m\left[-m^2 k_2^4 + 2(m^2 - 1) k_2^2 + k_2^{2-2m} + k_2^{2m+2} - m^2\right] \qquad (106)$$

The bending solution is found in a similar manner to the method used previously for the ring segment. The resulting total stresses and displacements for the pin segment are given in Equations (22a-c) and (23a, b) in the text. The functions $g_{m1}(r)$, $g_{m2}(r)$, and $g_{m3}(r)$ in Equations (22a-c) are recognized as the coefficients of $\cos m\theta$ and $\sin m\theta$ in Equations (103a-c). $g_{m4}(r)$ and $g_{m5}(r)$ in Equations (23a, b) are defined as:

$$g_{m4} \equiv -m(1+\nu) a_m \rho^{m-2} + \left[2(1-\nu) - m(1+\nu)\right] b_m \rho^m$$
$$+m(1+\nu) c_m \rho^{-m-2} + \left[2(1-\nu) + m(1+\nu)\right] d_m \rho^{-m}$$

$$g_{m5} \equiv m(1+\nu) a_m \rho^{m-2} + m\left[\frac{m+4}{m} + \nu\right] b_m \rho^m \qquad (107a, b)$$
$$+m(1+\nu) c_m \rho^{-m-2} + m\left[\frac{m-4}{m} + \nu\right] d_m \rho^{-m}$$

and G_2 is defined as

$$G_2 \equiv \frac{r_o}{E}\left\{ m(1+\nu) a_m \left(\frac{r_o}{r_2}\right)^{m-2} - \left[2(1-\nu) - m(1+\nu)\right] g_m \left(\frac{r_o}{r_2}\right)^m \right.$$
$$\left. -m(1+\nu) c_m \left(\frac{r_o}{r_2}\right)^{m-2} - \left[2(1-\nu) + m(1+\nu)\right] d_m \left(\frac{r_o}{r_2}\right)^{-m} \right\} \qquad (107c)$$

where

$$r_o = \frac{r_1 + r_2}{2} .$$

The bending moment is $M_2 p_1 r_1^2$ where

$$M_2 = \frac{1}{k_2^2 - 1}\left[\frac{k_2^2 - 1}{2} + k_2^2 \log k_2\right] + p_2\left[\frac{k_2^2}{2} + \frac{k_2^2 \log k_2}{k_2^2 - 1}\right]$$

$$+ \frac{1}{p_1}\left\{ - (m - 1)\, a_m\, k_2^{-m+2}\left[k_2^m - 1\right] - (m + 1)\, b_m\, k_2^{-m}\left[k_2^{m+2} - 1\right]\right.$$

$$\left. + (m + 1)\, c_m\, k_2^{m+2}\left[k_2^{-m} - 1\right] - (m - 1)\, d_m\, k_2^m\left[k_2^{-m+2} - 1\right]\right\} \qquad (108)$$

β_1 was defined previously by Equation (95).

The equations for stresses and deflections in pin segments were programmed on the computer and some calculations were carried out. Table LVII gives some results for $k_2 = 4.0$ and $\alpha = 60°$. At $\theta = \alpha/4 = 15°$ and $r/r_1 = 4$, edge of pin hole, it is noted that $\sigma_\theta/p_1 = 2.01$. This indicates the stress concentration effect of the hole. At $\theta = \alpha/2 = 30°$ appreciable σ_θ stress remains. The edge of the segment should be free of stress. Therefore, the results must be considered approximate. However, the residual σ_θ stress on the edge is self equilibrating and its removal would be expected to cause only a local effect near the edge according to the St. Venant principle.

Bending of the pin segment again is evident as shown by the v displacement. The variation of displacements and of the maximum σ_θ stress at the hole with segment geometry are shown in Table LVIII. Larger u displacements and smaller hoop stresses are found for larger k_2 and α. The bending displacement v increases with α but decreases with k_2.

The bending of pin segments would cause the inside corners to dig into the liner just as in the ring segments (Figure 78a). Therefore, an inside diameter of the segments larger than the outside diameter of the liner would again be recommended to counteract the bending effect.

SOLUTION FOR SHEAR STRESSES IN PINS

The pins of the pin-segment container are subject to shear and bending as shown in Figure 81. The shear stress is larger than the bending stress and will be used as the critical stress in the pins. The maximum shear stress in a circular pin is given by

$$\tau_{max} = \frac{4}{3A}(P/2)$$

TABLE LVII. STRESSES AND DEFLECTIONS IN A PIN SEGMENT, $k_2 = 4.0$, $\alpha = 60°$, $\nu = 0.3$

RESULTS AT THETA = 0.00 DEGREES

R/R1	SIGMA R/P1	SIGMA THETA/P1	TAU RTHETA/P1	FU/RP1	EV/RP1
1.000	-1.0000	-0.2009	0.0000	1.1739	0.0000
1.250	-0.8356	-0.1524	0.0000	0.7673	0.0000
1.500	-0.7174	-0.0967	0.0000	0.5167	0.0000
1.750	-0.6256	-0.0415	0.0000	0.3502	0.0000
2.000	-0.5522	0.0122	0.0000	0.2335	0.0000
2.250	-0.4948	0.0657	0.0000	0.1482	0.0000
2.500	-0.4555	0.1221	0.0000	0.0833	0.0000
2.750	-0.4409	0.1841	0.0000	0.0310	0.0000
3.000	-0.4598	0.2472	0.0000	-0.0143	0.0000
3.250	-0.5169	0.2840	0.0000	-0.0567	0.0000
3.500	-0.5954	0.2088	0.0000	-0.0980	0.0000
3.750	-0.6186	-0.1929	-0.0000	-0.1336	0.0000
4.000	-0.3755	-1.3937	-0.0000	-0.1456	0.0000

RESULTS AT THETA = 15.00 DEGREES

R/R1	SIGMA R/P1	SIGMA THETA/P1	TAU RTHETA/P1	FU/RP1	EV/RP1
1.000	-1.0000	-0.2009	0.0000	1.1048	-0.2753
1.250	-0.8355	-0.1525	0.0000	0.7120	-0.1703
1.500	-0.7169	-0.0972	0.0000	0.4707	-0.1003
1.750	-0.6236	-0.0433	0.0000	0.3109	-0.0503
2.000	-0.5449	0.0058	0.0000	0.1998	-0.0128
2.250	-0.4731	0.0478	0.0000	0.1202	0.0164
2.500	-0.3997	0.0797	0.0000	0.0625	0.0397
2.750	-0.3145	0.0998	0.0000	0.0218	0.0588
3.000	-0.2058	0.1129	0.0000	-0.0046	0.0747
3.250	-0.0670	0.1471	0.0000	-0.0178	0.0882
3.500	0.0863	0.2888	0.0000	-0.0202	0.0997
3.750	0.1788	0.7530	-0.0000	-0.0188	0.1097
4.000	-0.0000	2.0126	-0.0000	-0.0339	0.1185

TABLE LVII. (Continued)

RESULTS AT THETA = 22.50 DEGREES

R/R1	SIGMA R/P1	SIGMA THETA/P1	TAU RTHETA/P1	EU/RP1	EV/RP1
1.000	-1.0000	-0.2009	-0.0000	1.0195	-0.4018
1.250	-0.8356	-0.1524	-0.0000	0.6437	-0.2465
1.500	-0.7171	-0.0970	-0.0002	0.4138	-0.1430
1.750	-0.6246	-0.0424	-0.0010	0.2620	-0.0691
2.000	-0.5486	0.0090	-0.0034	0.1567	-0.0139
2.250	-0.4839	0.0567	-0.0099	0.0809	0.0285
2.500	-0.4276	0.1009	-0.0245	0.0249	0.0613
2.750	-0.3777	0.1419	-0.0527	-0.0172	0.0866
3.000	-0.3328	0.1800	-0.0971	-0.0494	0.1057
3.250	-0.2920	0.2156	-0.1467	-0.0742	0.1219
3.500	-0.2545	0.2488	-0.1504	-0.0933	0.1436
3.750	-0.2199	0.2800	0.0371	-0.1082	0.1915
4.000	-0.1877	0.3094	0.7577	-0.1197	0.3124

RESULTS AT THETA = 30.00 DEGREES

R/R1	SIGMA R/P1	SIGMA THETA/P1	TAU RTHETA/P1	EU/RP1	EV/RP1
1.000	-1.0000	-0.2009	-0.0000	0.9021	-0.5149
1.250	-0.8356	-0.1524	-0.0000	0.5498	-0.3120
1.500	-0.7174	-0.0967	-0.0000	0.3355	-0.1768
1.750	-0.6256	-0.0415	-0.0000	0.1948	-0.0801
2.000	-0.5522	0.0122	-0.0000	0.0976	-0.0077
2.250	-0.4948	0.0657	-0.0000	0.0274	0.0487
2.500	-0.4555	0.1221	-0.0000	-0.0255	0.0938
2.750	-0.4409	0.1841	-0.0000	-0.0678	0.1307
3.000	-0.4598	0.2472	-0.0000	-0.1049	0.1614
3.250	-0.5169	0.2840	-0.0000	-0.1404	0.1874
3.500	-0.5954	0.2088	-0.0000	-0.1757	0.2097
3.750	-0.6186	-0.1929	0.0000	-0.2061	0.2290
4.000	-0.3755	-1.3937	0.0000	-0.2135	0.2459

TABLE LVIII. DISPLACEMENTS AND MAXIMUM HOOP STRESSES IN PIN SEGMENTS, $\nu = 0.3$

k_2	σ_θ/p_1 at $\theta = \alpha/4$, $r = r_2$	$\frac{Eu}{rp_1}$ at $\theta = 0$		$\frac{Ev}{rp_1}$ at $\theta = \alpha/2$	
		$r = r_1$	$r = r_2$	$r = r_1$	$r = r_2$
		(a) $\alpha = 60°$			
2.0	4.3266	1.0074	-0.0151	-0.6387	0.5367
3.0	2.7247	1.0681	-0.1303	-0.5313	0.3202
4.0	2.0126	1.1739	-0.1456	-0.5149	0.2459
5.0	1.6019	1.2865	-0.1397	-0.4068	0.2554
		(b) $k_2 = 3.0$			
α					
45°	3.3815	1.0516	-0.1281	-0.4082	0.2336
60°	2.7247	1.0681	-0.1303	-0.5313	0.3202
90°	2.0820	1.1137	-0.1305	-0.7382	0.5195

where A is the area of the pin and P/2 is the shear force shown in Figure 81. For $A = \frac{\pi d^2}{4}$ (d is pin diameter) and P given by Equation (101), the maximum shear stress becomes

$$\tau_{max} = \frac{16}{3} \frac{p_1 r_1 t}{\pi d^2} \tag{109}$$

This equation is the basis of Equation (69) in the text.

APPENDIX II

DERIVATIONS OF FORMULAS FOR ASSEMBLY INTERFERENCES

The interferences Δ_n calculated in the text are the interferences required on the component parts as manufactured. However, the manufactured interference is not equal to the interference as assembled. The multiring container is taken as an example. It is assumed the rings are shrink-fit assembled one-by-one from the inside. The outer rings expand as they are shrunk on and the assembly interference for the next ring to be fitted is increased beyond the manufactured interference. The assembly interference between cylinders n and n + 1 is denoted by δ_n. It has dimensions of inches.

For assembly of cylinder n + 1 onto the other cylinders, δ_n is expressed as

$$\frac{\delta_n}{r_n} = \frac{\Delta_n}{r_n} + \frac{u'_n(r_n)}{r_n} \tag{110}$$

where

$u'_n(r_n)$ = radial displacement at r_n of cylinder n due to residual pressure q'_{n-1} at r_{n-1}.

q'_{n-1} = residual pressure at r_{n-1} due to assembly of cylinder n of wall ratio k_n onto a compound cylinder of wall ratio $k_1 k_2 \cdots k_{n-1}$ with an interference δ_{n-1}.

q'_{n-1} is calculated as follows:

$$\frac{\delta_{n-1}}{r_{n-1}} = \frac{u_n(r_{n-1}) - u_{n-1}(r_{n-1})}{r_{n-1}}$$

Substitution for u_n and u_{n-1} from Equation (14a) gives

$$\frac{\delta_{n-1}}{r_{n-1}} = \frac{1}{E_n(k_n^2-1)}\left[(1-v)\, q'_{n-1} + (1+v)\, q'_{n-1}\, k_n^2\right]$$

$$- \frac{1}{E_{n-1}(k_{n-1}^2\, k_{n-2}^2 \cdots k_1^2 - 1)}\left[-(1-v)\, q'_{n-1}\, k_{n-1}^2\, k_{n-2}^2 \cdots k_1^2 - (1+v)\, q'_{n-1}\right]$$

$$= \frac{q'_{n-1}}{E}\left[\frac{k_n^2+1}{k_n^2-1} + \frac{k_{n-1}^2\, k_{n-2}^2 \cdots k_1^2 + 1}{k_{n-1}^2\, k_{n-2}^2 \cdots k_1^2 - 1}\right]$$

where $E_n = E_{n-1} = E$ is assumed.

$$\text{Hence, } q'_{n-1} = E\left(\frac{\delta_{n-1}}{r_{n-1}}\right)\frac{\left(k_n^2-1\right)\left(k_{n-1}^2\, k_{n-2}^2 \cdots k_1^2-1\right)}{2\left(k_n^2\, k_{n-1}^2\, k_{n-2}^2 \cdots k_1^2 - 1\right)} \tag{111}$$

Since

$$\frac{u'_n(r_n)}{r_n} = \frac{2\,q'_{n-1}}{E\left(k_n^2-1\right)} \tag{112}$$

Substitution of (111) and (112) into (110) gives

$$\frac{\delta_n}{r_n} = \frac{\Delta_n}{r_n} + \frac{\delta_{n-1}}{r_{n-1}}\frac{\left(k_{n-1}^2\, k_{n-2}^2 \cdots k_1^2 - 1\right)}{\left(k_n^2\, k_{n-1}^2\, k_{n-2}^2 \cdots k_1^2 - 1\right)} \tag{113}$$

Now the $\frac{\delta_n}{r_n}$ can be calculated in sequence; i.e.,

$$\frac{\delta_1}{r_1} = \frac{\Delta_1}{r_1}$$

$$\frac{\delta_2}{r_2} = \frac{\Delta_2}{r_2} + \frac{\delta_1}{r_1}\frac{\left(k_1^2 - 1\right)}{\left(k_1^2\, k_2^2 - 1\right)} \quad \text{, etc.}$$

Equation (113) applies if the rings are assembled from the inside out. If the rings are assembled one by one from the outside in, then the assembly interference for assembly of cylinder n-1 into the other cylinders is

$$\frac{\delta_n}{r_n} = \frac{\Delta_n}{r_n} + \frac{\delta_{n+1}}{r_{n+1}}\,\frac{k_n^2 + 1}{\left(k_{n+1}^2\, k_{n+2}^2 \cdots k_N^2 - 1\right)}\,\frac{\left(k_{n+1}^2\, k_{n+2}^2 \cdots k_N^2 - 1\right)}{\left(k_{n+1}^2 k_{n+2}^2 \cdots k_N^2 - 1\right)} \tag{114}$$

Equation (114) was found by an analogous procedure to that used in deriving (113).

The method used to determine assembly interferences δ_n for the multiring container can also be used to determine assembly interferences for the other container designs. It is important to determine assembly interferences because they are larger than the manufactured interferences and excessive interference requirements may make a design impracticable.

APPENDIX III

COMPUTER PROGRAMS

The analyses described in the text were programmed in the FORTRAN IV alogarithmic language for calculation on Battelle's CDC 3400 and 6400 computers.* The following is a list of programs which includes a brief description of each:

PROGRAM COMPST1 – Analysis of compound (multi-ring) cylinder based upon static shear strength. Calculation of pressure-to-strength ratio p/2S in Figure 43 in the text.

PROGRAM COMPFG1 – Analysis of compound cylinder based upon shear fatigue strength. Calculation of pressure-to-strength ratio p/σ shown in Figure 44.

PROGRAM SEGMENT1 – Analysis of ring segment under radial pressures. Some results given in Appendix I.

PROGRAM SEGM2N – Analysis of pin segment under radial pressures and shear. Some results given in Appendix I.

PROGRAM COMPHS1 – Analysis of compound cylinder with high-strength liner. Calculations of pressure-to-strength ratios p/σ_1 and p/σ shown in Figures 45, 46, 47, and 48.

PROGRAM COMPHS2 – Analysis of compound cylinder with high-strength liner. Calculation of shrink-fit interferences, operating stresses, and prestresses.

PROGRAM PLTR1 – Analysis of Poulter (ring-segment) cylinder with high-strength liner. Calculation of pressure-to-strength ratios p/σ_1 and p/σ shown in Figures 49, 50, 51, and 52.

PROGRAM PLTR2 – Analysis of Poulter cylinder or pressure support cylinder (inner part of ring-fluid-segment container). Calculation of interferences, operating stresses, and prestress.

PROGRAM PSCYL1 – Analysis of pressure support cylinder (inner part of ring-fluid-segment container). Calculation of pressure-to-strength ratios p/σ_1 and p/σ_3 shown in Figures 53, 54, 55, 56, and 57.

PROGRAM PGSPNCYL – Analysis of segmented shear-pin (pin-segment) cylinder with high-strength liner. Calculation of pressure-to-strength ratio p/σ_1 and p_1/p shown in Figures 58 and 59.

PROGRAM MULTIR – General analysis of compound (multiring) cylinder based on fatigue-strength criterion. The program may be used interchangeably for the ring-fluid-ring design concept.

*Since writing the early programs, the CDC 3400 computer has been superceded by the more versatile CDC 6400 computer. The codes have been modified accordingly.

REFERENCES FOR VOLUME II

(20) Fiorentino, R. J., Abramowitz, P. H., Sabroff, A. M., and Boulger, F. W., "Development of the Manufacturing Capabilities of the Hydrostatic Extrusion Process", Interim Engineering Progress Report No. IR-8-198 (III), Contract No. AF 33(615)-1390 (August, 1965).

(21) Fiorentino, R. J., Gerdeen, J. C., Hansen, W. R., Sabroff, A. M., and Boulger, F. W., "Development of the Manufacturing Capabilities of the Hydrostatic Extrusion Process", Interim Engineering Progress Report No. IR-8-198 (IV), Contract No. AF 33(615)-1390 (December, 1965).

(22) Fiorentino, R. J., Gerdeen, J. C., Hansen, W. R., Sabroff, A. M., and Boulger, F. W., "Development of the Manufacturing Capabilities of the Hydrostatic Extrusion Process", Interim Engineering Progress Report No. IR-8-198 (V), Contract No. AF 33(615)-1390 (March, 1966).

(23) Manning, W. R. D., "High Pressure Engineering", University of Nottingham, Bulleid Memorial Lectures, Vol II, Lecture II, Chapter 4 (1963).

(24) Manning, W. R. D., "The Design of Compound Cylinders for High Pressure Service", Engineering, pp 349-352 (May 2, 1947).

(25) Manning, W. R. D., "Residual Contact Stresses in Built-Up Cylinders", Engineering, p 464 (December 8, 1950).

(26) Poulter, T. C., "High Pressure Apparatus", U. S. Patent No. 2,554,499 (May 9, 1951), Code No. P67.35, Annotated Bibliography on High Pressure Technology, ASME, Butterworths (May, 1964).

(27) Ballhausen, C., German Patent No. 1,142,341 (January 17, 1963).

(28) Gerard, G., and Brayman J., "Hydrostatic Press for an Elongated Object", Barogenics, Inc., U. S. Patent No. 3,091,804 (June 4, 1963).

(29) Fuchs, F. J., Jr., "Production Metal Forming With Hydrostatic Pressures", Western Electric Company, ASME Publication No. 65-PROD-17 (June 1965).

(30) Zeitlin, Alexander, Brayman, J., and Boggio, F. George, "Isostatic and Hydrostatic Equipment for Industrial Applications of Very High Pressure", ASME Paper No. 64-WA/PT-14.

(31) Meissner, M., "Hydrostatic Pressure Device", U. S. Patent No. 3,224,042, Filed October 23, 1963, Patented December 21, 1965.

(32) Lengyel, B., and Alexander, J. M., "Pressure Vessels for Hydrostatic Extrusion", The Chartered Mechanical Engineer, pp 405-406 (September, 1966).

(33) Lengyel, B., Burns, D. J., and Prasad, L. V., "Design of Containers for a Semi-Continuous Hydrostatic Extrusion Production Machine", Preprint of paper presented at 7th Int. M.T.D.R. Conference, Univ. of Birmingham, 12th-16th September, 1966..

(34) Manson, S. S. and Hirschberg, M. H., "Fatigue Behavior in Strain Cycling in the Low and Intermediate Cycle Range", 10th Sagamore Army Materials Research Conference, Sagamore, New York (August 13-16, 1963).

(35) Morrison, J. L. M., Crossland, B., and Parry, J. C. S., "The Strength of Thick Cylinders Subjected to Repeated Internal Pressure", J. of Engineering for Industry, Trans. ASME, Series B, Vol 82, pp 143-153 (1960).

(36) Aerospace Structural Materials Handbook, Vol I, Table 3.051.

(37) Gilewicz, E. P., Fragetta, W. A., Mehra, V., and Krohn, R., "Research on the Binary Iron-Nickel Alloys With 20-25% Ni", ASD-TDR-62-996, Fig. 107 (June, 1964).

(38) Lunn, J. A., Sampson, H. B., Federico, A. M., and Macaulay, J. R., "Nickel Maraging Steels, Preliminary Investigation of 250 and 300 Bar", North American Aviation Report No. NA63H-202, pp 22-27 (March 15, 1963).

(39) Booth, E. T., Brodrick, R. F., Friesecke, B. P., and Schofield, B. H., "Fatigue and Dynamic Creep of High Strength Steels", ASD-TDR-62-480 (August, 1962).

(40) O'Connor, H. C. and Morrison, J. L. M., "The Effect of Mean Stress on the Push-Pull Fatigue Properties of an Alloy Steel", Int. Conf. on the Fatigue of Metals, Inst. of Mech. Engineers, London (September, 1956).

(41) Timoshenko, S. and Goodier, J. N., "Theory of Elasticity", 2nd Edition, McGraw-Hill, pp 58-59, 66-67 (1951).

(42) Berman, I., "Design and Analysis of Commercial Pressure Vessels to 500,000 psi", ASME Paper No. 65-WA/PT-1, to be published in Trans. ASME, J. Basic Engineering.

(43) Pugh, H. Ll. D., and Green, D., "The Effect of Hydrostatic Pressure on the Plastic Flow and Fracture of Metals", Proc. Instn. Mech. Engrs., Vol. 179, Pt. 1, No. 12, 1964-65, pp 415-437.

(44) Crossland, B., and Dearden, W. H., "The Plastic Flow and Fracture of a "Brittle" Material (Gray Cast Iron) With Particular Reference to the Effect of Fluid Pressure", Proc. Instn. Mech. Engrs. Vol. 182 (1958) p 805.

(45) Bridgman, P. W., "Studies in Large Plastic Flow and Fracture", McGraw-Hill, New York (1952).

(46) Davidson, T. E., Eisenstadt, R., and Reiner, A. N., "Fatigue Characteristics of Open-End Thick-Walled Cylinders Under Cyclic Internal Pressure", Watervliet Arsenal Technical Report WVT-RI-6216 (August, 1962).

(47) Fiorentino, R. J., Sabroff, A. M., and Boulger, F. W., "Investigation of Hydrostatic Extrusion". Final Technical Documentary Report No. AFWL-TD-64-372, Contract No. AF 33(600)-43328 (January, 1965).

(48) Coffin, L. F., Jr., "Thermal Stress and Thermal Stress Fatigue", Proceedings of the Society of the Experimental Stress Analysis, 15 (2), 117-130 (1958).

(49) Sachs, G., Sell, R., Brown, W. F., "Tension, Compression and Fatigue Properties of Several Steels for Aircraft Bearing Applications", Proc. ASMT, 59, 635 (1959).

Distribution List
(Contract No. AF 33(615)-1390)

AFML (MATB) (15 copies)
Attention Mr. G. A. Gegel
Wright-Patterson AFB, Ohio 45433

AFML (MAMP)
Attention Mr. K. Kojola
Wright-Patterson AFB, Ohio 45433

AFML (MAMP)
Attention Mr. V. DePierre
Wright-Patterson AFB, Ohio 45433

AFML (MAAM)
Attention Library
Wright-Patterson AFB, Ohio 45433

FTD
Attention TD-E2b
Wright-Patterson AFB, Ohio 45433

Defense Documentation Center (DDC) (20)
Cameron Station
5010 Duke Street
Alexandria, Virginia 22134

Air Force Systems Command
Attention SCR-2, Mr. Kniffen
Andrews Air Force Base
Washington 25, D. C.

Bureau of Naval Weapons
RRMA (Mr. T. Kearns)
Washington 25, D. C.

Commanding Officer
Attention Mr. S. V. Arnold,
Associate Director
Watertown Arsenal Laboratories
Watertown 72, Massachusetts

U. S. Atomic Energy Commission
Technical Information Services Extension
Attention Mr. Hugh Voress
P. O. Box 62
Oak Ridge, Tennessee

National Academy of Science
National Research Council
Div. of Eng. & Industrial Resources
Attention Mr. E. V. Bennett
Washington 25, D. C.

National Aeronautics & Space
Administration
Lewis Research Center
Attention Mr. George Mandel,
Chief, Library
21000 Brookpark Road
Cleveland, Ohio 44125

Los Alamos Scientific Laboratory
Attention Dr. John E. Hockett
Los Alamos, New Mexico

Mr. William Bruckart (Aerojet-General,
Azusa, California)
23617A Anza Avenue
Torrance, California 90505

U. S. Army Watervliet Arsenal
Attention Mr. T. E. Davidson
SWEWV-RDR
Watervliet, New York

Aerojet General Corporation
P. O. Box 296
Azusa, California

Aerojet General Corporation
Solid Rocket Department
P. O. Box 1947
Sacramento, California

Advanced Technology Laboratories
Division of American Standard
Attention Mr. W. C. Wolff,
Contracts Manager
369 Whisman Road
Mountain View, California

DISTRIBUTION LIST
(Continued)

AFFDL (FDTS)
Wright-Patterson AFB, Ohio 45433

AFFDL (FDTS/M Sgt. J. D. Ingram)
Wright-Patterson AFB, Ohio 45433

AFML (MAA/Dr. D. H. Cartolano)
Wright-Patterson AFB, Ohio 45433

AFML (MAA/Mr. J. Teres)
Wright-Patterson AFB, Ohio 45433

AFML (MAAM/Mr. C. L. Harmsworth)
Wright-Patterson AFB, Ohio 45433

AFML (MAMN/Mr. Tom Cooper)
Wright-Patterson AFB, Ohio 45433

AFML (MAMP/Mr. N. M. Geyer)
Wright-Patterson AFB, Ohio 45433

AFML (MAMN/ Mr. S. Inouye)
Wright-Patterson AFB, Ohio 45433

AFML (MAP/ Mr. Besancon)
Wright-Patterson AFB, Ohio 45433

AFML (MATF)
Wright-Patterson AFB, Ohio 45433

AFML (MAX/Dr. A. L. Lovelace)
Wright-Patterson AFB, Ohio 45433

ASD (ASFE/Lt. Bowen)
Wright-Patterson AFB, Ohio 45433

ASD (SEVS)
Wright-Patterson AFB, Ohio 45433

AUL
Maxwell AFB Alabama 36112

FTD (TDEWP)
Wright-Patterson AFB,
Ohio 45433

RTD (SETFS/Mr. J. F. Rosenkranz)
Wright-Patterson AFB, Ohio 45433

SEG (SEJDA)
Wright-Patterson AFB, Ohio 45433

Hq USAF (AFRSTC)
Washington, D. C. 20330

Hq USAF (AFXSAI)
Air Battle Analysis Center
Deputy Director of Plans for War Plans
Directorate of Plans, DCS/P&O
Washington, D. C. 20330

SEPDE
Wright-Patterson AFB, Ohio 45433

HQ USAF (AFCSAI)
Study Information Group
Assistant Chief of Staff for
Study and Analysis
Washington, D. C. 20330

Allegheny Ludlum Steel Corporation
Research Center
Attention Mr. E. G. Flynn,
Supervising Metallurgist,
Extruded Products
Brackenridge, Pennsylvania

Aluminum Company of America
ALCOA Building
Attention Mr. R. W. Andrews
Pittsburgh, Pennsylvania

Aluminum Company of America
Attention Mr. Frederick C. Pyne
1200 Ring Building
Washington, D. C.

Mr. Hubert J. Altwicker
Lebanon, Ohio

Fansteel Metallurgical Corporation
Attention Mr. R. W. Yancey, Manager,
Special Development Projects
Number One Tantalum Place
North Chicago, Illinois 60064

DISTRIBUTION LIST
(Continued)

Air Reduction Company
Central Research Department
Central Research Laboratories
Attention Mr. J. K. Hamilton
Murray Hill, New Jersey

Babcock & Wilcox Company
Attention Mr. James Barrett
Beaver Falls, Pennsylvania

Baldwin-Lima-Hamilton Corporation
Industrial Equipment Division
Attention Mr. B. Shalomith
Philadelphia, Pennsylvania 19142

AFML (MANF/Mr. J. H. Ross)
Wright-Patterson AFB, Ohio 45433

Mechanical Technology, Inc.
Attention Mr. Marshall Peterson
968 Albany Shaker Road
Latham, New York

Case Institute of Technology
Metallurgy Department
Attention Mr. S. V. Radcliffe
Cleveland, Ohio 44106

Defense Metals Information Center
Battelle Memorial Institute
505 King Avenue
Columbus, Ohio 43201

The Boeing Company
Attention Mr. A. E. White, Mgr.,
Manufacturing Development
Section
P. O. Box 3985
Seattle, Washington

Barogenics, Incorporated
Attention Mr. A. Zeitlin
50 MacQuesten Parkway South
Mount Vernon, New York 10550

The Brush Beryllium Company
Attention Mr John Estess
17876 St. Clair Avenue
Cleveland, Ohio 44110

The Brush Beryllium Company
Attention Mr R. G. O'Rourke
17876 St. Clair Avenue
Cleveland, Ohio 44110

Jet Propulsion Laboratory
California Inst. of Technology
Attention Mr. I. W. Newlan
4800 Oak Grove Drive
Pasadena 3, California

Canton Drop Forging & Mfg. Co.
Attention Mr. Chandis Brauchler
2100 Wilett Avenue
Canton, Ohio

Westinghouse Electric Company
Bettis Field
Pittsburgh, Pennsylvania
Attention Mr. Kermeth Goldman

Crucible Steel Company of America
Attention Dr. Walter Finley,
Director of Research
P. O. Box 88
Pittsburgh 30, Pennsylvania

Curtiss-Wright Corporation
Metals Processing Division
Attention Mr. F. C. Wagner
760 Northland Avenue
Buffalo 15, New York

Curtiss-Wright Corporation
Wright-Aeronautical Division
Attention Mr. R. J. Moran,
Manager, Manufacturing
Engineering
Wood-Ridge, New Jersey

Douglas Aircraft Company, Inc.
Attention Mr. L. J. Devlin
Materials Research & Process
Santa Monica, California

DISTRIBUTION LIST
(Continued)

Dow Chemical Company
Metallurgical Laboratory
Attention Dr. T E. Leontis,
Assistant to the Director
Midland, Michigan

E. I. du Pont de Nemours & Company
Pigments Department
Attention Colin I. Bradford,
Director - Metals Products
Wilmington, Delaware 19898

E. I. du Pont de Nemours & Company,
Incorporated
Du Pont Metals Center
Attention Dr. L. J. Klinger
Baltimore, Maryland

Chance Vought Corporation
Vought Aeronautics Division
Attention Mr. G. A. Starr
P. O. Box 5907
Dallas, Texas

Alpha Metals, Inc.
Attention Mr. R. H. Hilsinger
56 Water Street
Jersey City, New Jersey 07304

Douglas Aircraft Company, Inc.
Attention Mr. C. B. Perry, C-345,
Plant Engineering Supervisor
3855 Lakewood Boulevard
Long Beach, California 90808

E. I. du Pont de Nemours & Company,
Incorporated
Engineering Research Laboratory
Attention Mr. Donald Warren
Wilmington 98, Delaware

Erie Foundry Company
Attention Mr. J. E. Wilson
General Sales Manager
Erie 6, Pennsylvania

General Hefco Corporation
3030 Bryan
Fort Worth, Texas 76110
Attention Mr. Richard H. Wesley

Fansteel Metallurgical Corp.
Attention Mr. A. B. Michael,
Director, Metallurgical
Research
2200 Sheridan Road
North Chicago, Illinois

Feller Engineering Company
Attention Mr. R. C. Zeile
Empire Building
Pittsburgh, Pennsylvania

General Electric Company
Aircraft Gas Turbine Division
Attention Mr. G. J. Wile
Engineering Manager,
Metallurgical Engineering
Operations
Large Jet Engine Department
Building 501
Cincinnati 15, Ohio

Grumman Aircraft Engineering
Corporation
Manufacturing Engineering
Attention Mr. W. H. Hoffman,
Vice President
Plant 2
Bethpage, Long Island, New York

High Pressure Data Center
P. O. Box 60, University Station
Brigham Young University
Provo, Utah 86601

IIT Research Institute
Metals Research Department
Attention Dr. W. Rostoker
10 West 35th Street
Chicago, Illinois 60616

General Electric Company
F. P. D. Technical Information
Center
Building 100
Cincinnati 15, Ohio

DISTRIBUTION LIST
(Continued)

General Astrometal Corporation
Attention Mr. L. Smiley
320 Yonkers Avenue
Yonkers, New York

General Cable Corporation
Research Laboratory
Attention Mr. J. Szilard,
Director of Research
Bayonne, New Jersey

General Dynamics/Fort Worth
Attention P. R. de Tonnaneour,
Chief Librarian
P. O. Box 748
Fort Worth, Texeas 76101

R. K. May
Chief of Applied Manufacturing
Research and Process Development
General Dynamics/Fort Worth
Fort Worth, Texas 76101

General Dynamics Corporation
Attention H. Richard Thornton
P. O. Box 748
Fort Worth, Texas 76101

General Dynamics
Attention Mr. F. H. Crane
P. O. Box 748
Fort Worth, Texas 76101

General Electric Company
Attention Library, LMC Department
1331 Chardon Road
Cleveland 17, Ohio

H. M. Harper Company
Attention Mr. K. G. Hookanson,
General Manager, Metals Division
Lehigh Avenue and Oakton Street
Morton Grove, Illinois

Harvey Aluminum, Inc.
Attention Mr. G. A. Moudry,
Technical Director
19200 South Western Avenue
Torrance, California

Haynes Stellite Company
Division of Union Carbide Corp.
Attention Mr. G. A. Fritzlen,
Manager, Technology
Kokomo, Indiana

Hunter Douglas Research Company
Attention Mr. Neal Gammell
887 East Second Street
Pomona, California 92505

Jones & Laughlin Steel Corp.
Attention Mr. Robert S. Orr,
Commercial Research Librarian
3 Gateway Center
Pittsburgh 30, Pennsylvania

Kaiser Aluminum & Chem. Corp.
1625 "I" Street, N. W.
Washington, D. C.

Lockheed Aircraft Corporation
Attention Mr. Green
Manufacturing Methods Division
Burbank, California

LaSalle Steel Company
Attention Mr. Elliot Nachtman
P. O. Box 6800-A
Chicago 80, Illinois

Lewis Research Center
Attention Capt. J. O. Tinius
AFSC/STLO
21000 Brookpark Road
Cleveland, Ohio

DISTRIBUTION LIST
(Continued)

The Ladish Company
Metallurgical Dept. Library
Attention Mr. Joseph Fischer
Cudahy, Wisconsin

Lehigh University
Attention Dr. Betzalel Avitzur, Assoc. Prof.
of Metallurgy and Material Science
Bethlehem, Pennsylvania

Watervliet Arsenal
Maggs Research Center
Attention Dr. T. A. Davidson
Watervliet, New York 12189

Kaiser Aluminum & Chemical Corp.
Dept. of Metallurgical Research
Attention Mr. T. R. Pritchett,
Assistant Director
Spokane, Washington 99215

U. S. Army Missile Command
AMSMR-RKK (Mr. Charles H. Martens)
Redstone Arsenal, Alabama

U. S. Army Materials Research Agency
Watertown Arsenal Laboratories
Attention Mr. Robert Colton
Chief, Shaping Technology Branch
Watertown, Massachusetts

New England Materials Laboratory, Inc.
Attention Mr. Attan S. Bufferd, Sc. D.
Mgr., Materials & Processes
35 Commercial Street
Medford, Massachusetts 02155

J. William Krohn
125 West 45th Street
New York, New York 10036

NASA-Marshall Space Flight Center
Redstone Arsenal
Attention Mr. William A. Wilson
Chief, Methods Development Branch, R-ME-MM
Manufacturing Research Technology Division
Huntsville, Alabama 35812

Westinghouse Electric Corporation
Attention David C. Goldberg
Manager, Materials Department
P. O. Box 80864
Pittsburgh, Pennsylvania 15236

Physmet Corporation
Attention Joseph S. Harvey
156 Sixth Street
Cambridge, Massachusetts 02142

Lockheed Missile and Space Co.
Attention Mr. Ronald L. Greene
Advanced Materials D81-31
P. O. Box 504
Sunnyvale, California

AFML (MAMP/K. Elbaum)
Wright-Patterson Air Force Base
Ohio 45433

General Dynamics
Electro Dynamics Division
Attention Warren G. Mang,
Product Manager
150 Avenel Street
Avenel, New Jersey

Monsanto Company
Development Dept.
Attention Mr. C. Early
800 N. Lindberg Boulevard
St. Louis, Missouri 63166

Proctor and Gamble Co.
Attention Dr. Robert E. Wann,
Chemical Derivatives
Ivory Dale-Technical Center
Cincinnati, Ohio 45217

General Electric Company
Metallurgy and Ceramics Laboratory
Attention D. W. Lillie, Manager
Metals Branch
P. O. Box 8
Schenectady, New York

DISTRIBUTION LIST
(Continued)

Magnethermic Corporation
Attention Mr. J. A. Logan
Youngstown, Ohio

The Martin Company
Attention Mr. L. Laux, Chief,
Manufacturing Research & Development
Baltimore 3, Maryland

The Martin Company
Denver Division
Attention Mr. R. F. Breyer,
Materials Engineering
Mail No. L-8, P. O. Box 179
Denver 1, Colorado

Marquardt Aircraft Corporation
16555 Saticoy Street
P. O. Box 2013 South Annex
Van Nuys, California

McDonnell Aircraft Corporation
Lambert-St. Louis Municipal Airport
Attention Mr. H. Siegel
P. O. Box 516
St. Louis 3, Missouri

North American Aviation, Inc.
Attention Mr. Walter Rhineschild
International Airport
Los Angeles, California 90045

Nuclear Metals, Inc.
Attention Mr. Klein, Vice President
Concord, Massachusetts

National Forge Company
Attention Mr. James R. Beckser,
Project Engineer
Press Form Products
Irvine, Warren County, Pennsylvania

Oregon Metallurgical Corporation
Attention Mr. F. H. Vandenburgh,
Vice President & Sales Manager
P. O. Box 484
Albany, Oregon

Kennecott Copper Corporation
Ledgemont Laboratory
Attention Mr. Stanley H. Gelles
128 Spring Street
Lexington 73, Massachusetts

Republic Aviation Corporation
Attention Mr. A. Kastelowitz,
Director of Manufacturing Research
Farmingdale, Long Island, New York

Republic Steel Corporation
Republic Research Center
6801 Brecksville Road
Cleveland 31, Ohio

Reynolds Metals Company
503 World Center Building
Washington 6, D. C.
Attention Mr. Stuart Smith

Rohr Aircraft Corporation
Attention Mr. F. E. Zinnerman,
Manager, Manufacturing Research
P. O. Box 878
Chula Vista, California

Ryan Aeronautical Company
Attention Mr. L. J. Hull, Chief
Metallurgist
Materials & Process Laboratory
Lindberg Field
San Diego 12, California

Reading Tube Corporation
Attention Mr. Griffith Williams, Jr.
P. O. Box 126
Reading, Pennsylvania 19603

Western Electric Company
Engineering Research Center
Attention Mr. Frank J. Fuchs, Jr.
Princeton, New Jersey

DISTRIBUTION LIST
(Continued)

Sandia Corporation
Livermore Laboratory
Attention Mr. M. W. Mote, Jr.
P. O. Box 969
Livermore, California

Solar Aircraft Company
A Division of International
Harvester Company
Attention Librarian
2200 Pacific Avenue
San Diego 12, California

National Aeronautics & Space
Administration
Lewis Research Center
Attention Mr. C. P. Blankenship
M. S. 105-1
21000 Brookpark Road
Cleveland, Ohio 44135

Ravens-Metal Products, Inc.
Attention Mr. Lloyd A. Cook
P. O. Box 1385
Parkersburg, West Virginia

Voi-Shan Manufacturing Company
Technical Sales Department
Attention Mrs. Virginia Kuidroff
8463 Higuera Street
Culver City, California

Reynolds Metals Company
Attention Mr. J. Harry Jackson,
General Director
Metals Research Division
Richmond, Virginia

Allis-Chalmers
Attention Dr. Laird C. Towle,
Research Physicist
Box 512
Milwaukee, Wisconsin 53201

GCA Viron Division
Attention Mr. W. H. Schaumberg,
Manager
Instrumentation and Communication
7585 Viron Road, N. E.
Minneapolis, Minnesota 55432

Mr. W. B. Aufderhaar, Manager
Technical Service
Special Metals Corporation
New Hartford, New York 13413

Titanium Metals Corporation of
America
Attention Mr. W. M. Parris,
Senior Research Engineer
P. O. Box 2128
Henderson, Nevada 89015

J. Bishop & Co., Platinum Works
Attention Supervisor, Production
Engineering
Malvern, Pennsylvania

GM Defense Research Laboratories
Box T
Santa Barbara, California
Attention Dr. Arfon H. Jones,
Materials and Structures
Laboratory

Western Electric Company
Attention Mr. Fred Radakovich,
Senior Staff Engineer
Dept. 7224, Hawthorne Station
Chicago, Illinois 60623

Eaton Yale & Towne, Inc.
Research Center
Attention Library
26201 Northwestern Highway
Southfield, Michigan 48076

Sunstrand Aviation-Rockford
Attention R. W. Diesner, 763 M
2421 11th Street
Rockford, Illinois 61101

DISTRIBUTION LIST
(Continued)

The Beryllium Corporation
Attention Mr. E. C. Bishop
Reading, Pennsylvania

Astrosystems International, Inc.
Attention Mr. Robert F. Strauss,
Vice President
1275 Bloomfield Avenue
Fairfield, New Jersey 07007

The Beryllium Corporation
Attention E. A. Smith, Jr.,
Assistant to the Vice President
Reading, Pennsylvania 19603

Alcan Metal Powders, Inc.
Attention D. O. Noel, President
P. O. Box 290
Elizabeth, New Jersey 07207

Gulf States Tube Corporation
P. O. Box 952
Attention L. E. Branan,
Metallurgist
Rosenburg, Texas 77471

Commanding General
AMSEL-KL-EM (Dr. DiVita)
Ft. Monmouth, New Jersey 07703

Thompson-Ramo-Wooldridge, Inc.
Staff Research & Development
Chemical & Metallurgical Department
Attention Mr. A. S. Nemy
23555 Euclid Avenue
Cleveland 17, Ohio

Texas Instruments Corporation
Metals & Controls
Attention Mr. J. Buchinski
34 Forest Street
Attleboro, Massachusetts 02703

United States Steel Corporation
Products Development Division
525 William Penn Place
Pittsburgh, Pennsylvania

Universal Cyclops Steel Corporation
Refractomet Division
Attention Mr. C. P. Mueller,
General Manager
Bridgeville, Pennsylvania

University of California
Los Alamos Scientific Laboratory
P. O. Box 1663
Los Alamos, New Mexico

United Aircraft Corporation
Research Laboratories
Attention Mr. H. Peter Barie
East Hartford, Connecticutt

Director, USAEL
Hq. USAECOM
Attention AMSEL RD-PEE
(Mr. Divita)
Ft. Monmouth, New Jersey 07703

Wah Chang Corporation
Attention Mr. K. C. Li, Jr.
233 Broadway
New York, New York

Wolverine Tube
Division of Calumet & Hecla, Inc.
Attention Mr. D. F. Grimm, Mgr.,
Special Metals, Research &
Development Division
17200 Southfield Road
Allen Park, Michigan

Jeffrey Manufacturing Company
271 East First Street
Columbus, Ohio 43216

Wyman-Gordon Company
Attention Mr. Arnold Rustay,
Technical Director
Grafton Plant
Worcester Street
North Grafton, Massachusetts

DISTRIBUTION LIST
(Continued)

Westinghouse Electric Corporation
Attention Mr. F. L. Orrell,
Section Manager, Development
Contracts
P. O. Box 128
Blairsville, Pennsylvania

Watervliet Arsenal
Process Engineering Section
Benet Laboratories
Attention Mr. Leonard Liuzzi
Watervliet, New York

Lombard Corporation
Attention Mr. Daniel A. Katko,
Vice President
639 Wick Avenue
P. O. Box 177
Youngstown 1, Ohio

SEPIE
Wright-Patterson AFB, Ohio

SEPIR
Wright-Patterson AFB, Ohio

Clevite Corporation
Attention Mr. Gail F. Davies
540 East 105th Street
Cleveland 8, Ohio

Sun Oil Company
Attention Mr. E. M. Kohn
Marcus Hook, Pennsylvania

General Electric Company
Attention Mr. W. C. Gutjahr
118 W. First Street
Dayton, Ohio 45402

Pressure Technology Corporation of
America
Attention Dr. A. Bobrowsky
Boalsburg, Pennsylvania 16827

Brunswick Corporation
Corporate Research & Development
Needham Laboratories
Needham, Massachusetts 02192

IIT Research Institute
10 West 35 Street
Chicago, Illinois 60616

General Motors Corporation
Manufacturing Development
GM Technical Center
Attention Mr. J. W. Kusiak,
Dept. 30
Warren, Michigan 48090

General Electric Company
Atomic Power Equipment Dept.
Attention Library
175 Curtner Avenue
San Jose, California 95125

IIT Research Institute
Attention Asst. Director
Mechanics Research Division
10 West 35th Street
Chicago, Illinois 60616

Oak Ridge National Laboratory
Attention Mr. W. R. Martin
Building 4508
Oak Ridge, Tennessee

Norris Industries
P. O. Box 58507, Vernon Branch
5215 South Boyle Avenue
Los Angeles, Calif. 90058

Sandia Corporation
Attention Mr. D. R. Adolphson-Org
1131
Sandia Base
Albuquerque, New Mexico 87115

DISTRIBUTION LIST
(Continued)

Hq USAF(AFSPDI/Mr. W. Martin)
The Pentagon
Washington, D. C. 20330

Phelps Dodge
Aluminum Products Corporation
Rod Plant
P. O. Box D
Columbia, Tenn. 38401

Naval Air Systems Command
Attention Mr. R. Schmidt
Department of the Navy
Code AIR 520311
Washington, D. C. 20360

Harwood Engineering Co.
Attention Mr. D. Newhall, President
South Street
Walpole, Massachusetts

UNCLASSIFIED

Security Classification

DOCUMENT CONTROL DATA - R & D

(Security classification of title, body of abstract and indexing annotation must be entered when the overall report is classified)

1. ORIGINATING ACTIVITY (Corporate author)	2a. REPORT SECURITY CLASSIFICATION
Battelle Memorial Institute Columbus Laboratories Columbus, Ohio 43201	Unclassified
	2b. GROUP

3. REPORT TITLE

DEVELOPMENT OF THE MANUFACTURING CAPABILITIES OF THE HYDROSTATIC EXTRUSION
VOL. I AND II

4. DESCRIPTIVE NOTES (Type of report and inclusive dates)

TECHNICAL REPORT (FINAL) December 1964 - October 1967

5. AUTHOR(S) (First name, middle initial, last name)

Vol. I - Robert J. Fiorentino, Barry D. Richardson, George E. Meyer, Alvin M. Sabroff, Francis W. Boulger
Vol. II - Robert J. Fiorentino, James C. Gerdeen, Barry D. Richardson, Alvin M. Sabroff, Francis W. Boulger

6. REPORT DATE	7a. TOTAL NO. OF PAGES	7b. NO. OF REFS
October 1967	258	49

8a. CONTRACT OR GRANT NO.	9a. ORIGINATOR'S REPORT NUMBER(S)
AF 33(615)-1390	AFML-TR-67-327
b. PROJECT NO. 8-198	
c.	9b. OTHER REPORT NO(S) (Any other numbers that may be assigned this report)
d.	--

10. DISTRIBUTION STATEMENT This document is subject to special export controls and each transmittal to foreign governments or foreign nationals may be made only with prior approval of the Manufacturing Technology Division of the Air Force Materials Laboratory, Wright-Patterson Air Force Base, Ohio 45433.

11. SUPPLEMENTARY NOTES	12. SPONSORING MILITARY ACTIVITY
	Air Force Materials Laboratory Research and Technology Division, Air Force Systems Command, Wright-Patterson Air Force Base, Ohio

13. ABSTRACT

The effects of critical process variables on product quality and pressure requirements were investigated for wrought and powder material; 7075-0 aluminum, AISI 4340 steel, Ti-6Al-4V alloy, beryllium, TZM molybdenum alloy, S.A.P., Alloy 718, A286, Cb752. Products investigated were rounds, shapes, tubing and wire.

A study of general high pressure container designs has led to a better understanding of the design parameters to be applied for specific applications. A description of containers designed and constructed in this program is given.

This document is subject to special export controls and each transmittal to foreign governments or foreign nationals may be made only with prior approval of the Manufacturing Technology Division of the Air Force Materials Laboratory, Wright-Patterson Air Force Base, Ohio 45433.

DD FORM 1 NOV 65 1473

UNCLASSIFIED

14. KEY WORDS	LINK A		LINK B		LINK C	
	ROLE	WT	ROLE	WT	ROLE	WT
Hydrostatic extrusion						
Hydrostatic extrusion - Drawing						
Processing parameters						
Rounds, shapes and wire						
80 and 500 F						
AISI 4340 steel						
7075-0 aluminum						
Ti-6Al-4V alloy						
TZM molybdenum alloy						
Beryllium						
Alloy 718						
A286						
Sintered Aluminum Product (SAP)						
Hydrostatic extrusion containers						
Design						
Construction						
Evaluation						